

Aerial physical interaction with robust stability guarantee against sudden collision and contact-loss

Dongjae Lee, Jeonghyun Byun, and H. Jin Kim

Abstract—Aerial physical interaction (APhI) may incur unexpected collision or contact-loss due to uncertainty and unawareness of environment dynamics. Such contingencies should be carefully addressed and analyzed since they can deteriorate performance and even destabilize the interacting aerial robot. To this end, this work presents a complete hybrid system model valid throughout APhI with uncertain discontinuities in velocity and interaction wrench associated with unexpected collision and contact-loss. A disturbance-observer-based robust controller is then proposed to ensure robustness against continuous disturbance, and the closed-loop hybrid system is analyzed, showing further robustness against uncertain discontinuities. Next, we propose a motion planning algorithm ensuring practical safety with respect to rotor saturation while facilitating physical interaction. The proposed framework is demonstrated in five different experiment scenarios that include multiple occurrences of sudden collision and contact-loss: pushing a movable object 1) under unexpected change of friction, 2,3) colliding with another object, 4) on a slanted surface, and 5) with multiple contacts.

Index Terms—aerial physical interaction, impulsive switched system, hybrid system, disturbance-observer, input-to-state stability.

I. INTRODUCTION

Aerial physical interaction (APhI) has been an active research topic in recent decades [1, 2]. During APhI where a non-zero interaction wrench exists, an aerial robot may encounter various types of discontinuities. For example, imperfect estimation of the distance to a contact surface or surrounding obstacles incurs sudden collision which leads to a velocity jump [3, 4]. Furthermore, when an interacting object suddenly moves, an aerial robot experiences a jump in interaction wrench due to the discontinuous nature of the friction in the contact surface between the robot and the object or between the object and environment. Such discontinuity in interaction wrench becomes more apparent when sudden contact-loss happens, for instance, when an initially static interacting object slides down a slope after being pushed as in Fig. 1(c).

A. Problem description

In this work, we consider the problem of APhI with a possibly dynamic object where discontinuities by sudden collision or contact-loss may occur. Although recent works [5–7] consider similar task of pushing a possibly dynamic object, they mostly assume that no discontinuity in velocity

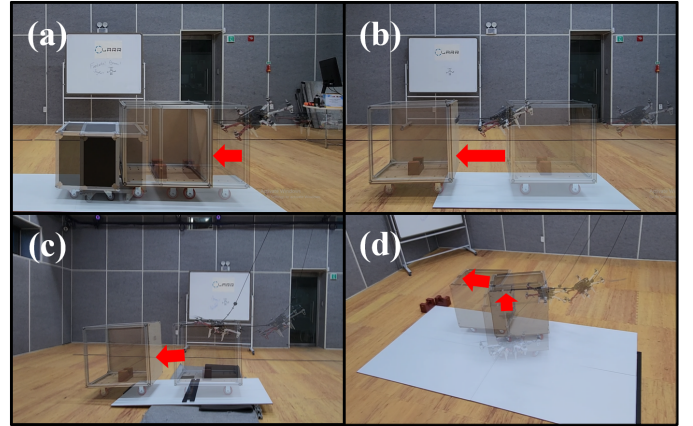


Fig. 1. Four different experiments showing robustness against sudden collision or contact-loss, representative phenomena including uncertain discontinuities in velocity and interaction wrench, during pushing a possibly dynamic object with unknown dynamics. A string connected to the robot is only for safety regulation.

or contact wrench exists; thus, robustness with respect to such discontinuities may not be guaranteed, and the performance can get degraded. One way to formally capture such discontinuities in a modeling process is to utilize a hybrid dynamical system [3, 8, 9]. There exist a few studies [4, 10–12] on aerial robots that adopt hybrid dynamical system to model aerial physical interaction. However, they have limitations in that discontinuities in velocity or interaction wrench are not addressed, and/or closed-loop stability is not analyzed with respect to all state variables.

Next, since it is difficult to predict the response of an unknown movable object to collision and to continuous interaction wrench exerted from an aerial robot, uncertainty should be considered in the system dynamics model. For example, if only perfectly plastic collision is taken into account as in [3, 13–15], the velocity after the collision can be modeled as zero and no uncertainty exists; however, because such simplification is not valid when interacting with a movable object and it is difficult to predict the response of the movable object to the collision, uncertainty is unavoidable in the velocity jump modeling.

Lastly, to autonomously and safely execute APhI of pushing an object with unknown physical parameters including mass, moment of inertia and friction model, a motion planning strategy should be 1) adaptive to overcome uncertainty of the object and 2) aware of physical limitation of the platform for safety. Since an object has unknown physical parameters, the magnitude of the interaction wrench required to make the object move is unknown. Furthermore, a pushing strat-

The authors are with the Department of Aerospace Engineering and the Automation and Systems Research Institute (ASRI), Seoul National University, Seoul 08826, South Korea (Corresponding author: H. Jin Kim) {ehdwo713, quswjdqus97, hjinkim}@snu.ac.kr

egy without due consideration may result in an excessive interaction wrench, especially when engaging with an object exhibiting motion constraints in specific directions or becoming wedged while being pushed. Although there exist a few pushing strategies for the APhI task [5, 7, 16–18], no work considers rotor saturation by excessive interaction wrench generation.

B. Objective and contribution

In the perspectives described above, the primary objective of this work is to provide robust stability guarantee of APhI even in the presence of an uncertain interaction model and unknown jumps in velocity and interaction wrench. To accomplish this objective, we first present a hybrid dynamical model of an aerial robot conducting physical interaction with a possibly dynamic object to encompass various APhI tasks. In contrast to existing models for APhI, the derived hybrid dynamical model is rich enough to capture discontinuities in velocity and interaction wrench and their instant occurrences that cannot be predefined with known timings. Since the models for friction and impact cannot be precisely identified before physical interaction, we allow uncertainties in modeling APhI as a hybrid system.

Next, we design a disturbance-observer (DOB)-based robust controller to provide robustness against model uncertainty and external disturbance. Compared with our previous work [5], we further modify the control structure to ensure that control inputs are well-defined regarding underactuatedness of conventional multirotors and to facilitate stability analysis of the overall hybrid system. Then, by representing the closed-loop system as an impulsive switched system and analyzing its stability, we verify that the aerial robot is robust not only to continuous disturbances but also to sudden contact-loss and collision incurring uncertain discontinuities in velocity and interaction wrench in unknown timings. Although the proposed methods are primarily designed considering underactuated aerial robots, our result is also applicable to fully actuated aerial robots with little modification.

In addition to the primary objective, our secondary objective is to design a saturation-aware pushing strategy during APhI of pushing a possibly dynamic object. By utilizing an estimate of the interaction force, we can avoid generation of an excessive interaction force and prevent rotor saturation. In addition, by integrating the proposed strategy with a path navigation algorithm, the proposed integrated motion planner enables an aerial manipulator to autonomously execute more complex APhI including sequential pushing of a possibly dynamic object while altering contact points as in Fig. 1 (d).

Finally, to demonstrate the proposed methods, we conduct extensive experiments: pushing a movable object 1) under unexpected change of friction, 2) colliding with another movable object, 3) colliding with a static environment, 4) on a slanted surface incurring sudden contact-loss, and 5) capable of both translation and rotation with multiple contacts. Through the experiments illustrated in Fig. 1, we successfully demonstrate effectiveness of the proposed framework.

To summarize, main contributions of this study are as follows:

- complete hybrid system modeling valid throughout APhI with possible jumps in velocity and interaction wrench
- robust controller design and closed-loop hybrid system stability analysis
- saturation-aware motion planning for APhI with a possibly dynamic object
- experimental validation involving pushing a movable object 1) under unexpected change of friction, 2,3) colliding with another object, 4) on a slanted surface incurring sudden contact-loss, and 5) capable of both translation and rotation with multiple contacts

II. RELATED WORK

A. System modeling for APhI

Considering kinematic constraint(s) existing during physical interaction, constrained system dynamics can be derived using Euler-Lagrange formulation as in [17, 19] or using quasi-steady state assumption as in [20]. However, relying on such a single constrained system dynamics model, system dynamics during no interaction or transition between non-interacting mode and interacting mode cannot be defined. This lack of richness in describing system dynamics may prevent proper controller design for the whole system and formal stability guarantee. Two equations of motion each describing non-interacting and interacting modes are introduced in [21, 22], but still such system dynamics representation cannot capture possible discontinuity occurring during the transition between the two modes. Another approach to model APhI is to allow an exogenous signal, i.e. an interaction wrench, to appear in the system dynamics [5, 7, 23–27]. However, since most of the works assume the interaction wrench to be continuous or even differentiable, their system analyses may not accord with a more general setting including an impulsive or discontinuous interaction wrench. Thus, a new system model is required that can cover multiple sets of equations of motion according to interacting and non-interacting modes and transitions among the modes that can capture discontinuity, while enabling system analysis to guarantee the stability of the system.

To handle such issues, a hybrid system [8] has been introduced to model APhI. However, existing works have limitations in that they either rely on simplified or linearized dynamics [4, 10] or consider only simple transition conditions [11, 12]. Unlike in general APhI where when and how often jumps in state or interaction wrench occur are unknown, [11] tackles only a known interaction wrench jump happening only once during a plug-pulling task, and [12] assumes to know the exact timing and model of a velocity jump. Since environment parameters including restitution coefficient are usually inaccessible in general, an exact velocity jump model is unknown. Therefore, to fully represent dynamic behavior of APhI, it is required to derive a system model that can 1) encompass full dynamics of an aerial robot, 2) accommodate flexibility in defining timing and frequency of mode transitions, and 3) involve uncertainty in system dynamics.

B. Control and stability analysis for APhI

The control objective is to enable an aerial manipulator to perform APhI while ensuring robustness against various

types of disturbance or uncertainty including near-wall effect, a robotic arm's motion, interaction wrench during APhI (if considered as a disturbance), and uncertain inertia of the aerial manipulator itself. Furthermore, we additionally aim to verify robustness to uncertain discontinuities in velocity and interaction wrench.

Although there exist various papers on controlling aerial manipulators [6, 7, 10, 20–24, 26], they either do not present stability analysis or do not tackle robustness against multiple types of disturbance or disturbance rejection property in their stability analysis. Thus, performance in the presence of a large, time-varying disturbance such as sudden robotic arm's motion with large amplitude or large interaction wrench would not be ensured and may easily get deteriorated. To ensure such robustness, various robust control techniques have been proposed [5, 28–31]. However, since they require an external disturbance to be continuous or even continuously differentiable while treating an interaction wrench as a disturbance, their stability analyses are no longer valid if an interaction wrench becomes discontinuous or impulsive.

To address robustness in the presence of discontinuous interaction wrench, [11, 32] design a robust switching controller for a task of pulling a wedged object. However, since distinguishing the exact controller switch timing is difficult in practice, and delayed controller switching may rather lead to instability [33], it would be demanding to ensure stability using a switching controller in the presence of multiple jumps with unknown timings. Therefore, to wholly satisfy the control objective, it is required to design a robust controller and provide stability guarantee while taking multiple jumps with unknown timings into account.

C. Pushing strategy for APhI with a possibly dynamic object

As one representative APhI task involving sudden collision and contact-loss, we perform pushing a possibly dynamic object using an aerial manipulator. Since physical parameters of the interacting object, such as mass, moment of inertia, and friction model, are usually unknown, methods assuming to know those physical parameters of the object [16, 17] may be impractical. Although [7] presents a pushing strategy where a constant reference is assigned for an interaction force, such strategy would fail if the predefined constant force reference is smaller than the maximum static friction of the object or may induce a large overshoot if the force reference is taken to be conservatively, excessively large. Therefore, a pushing strategy should be adaptive to the pushing object's state, either by directly or indirectly modulating the interaction wrench.

To achieve such adaptive nature, there have been strategies to design the interaction wrench with the object's position error [5, 6, 12, 21] or with a velocity error of the object [18, 19]. Although not presented in most papers, the underlying assumption of these strategies is that an aerial manipulator is capable of generating a sufficiently large interaction wrench that enables to overcome the maximum static friction of the object being pushed. However, in cases of the object being constrained in certain direction or the object being stuck in-between moving, these strategies may suffer from actuator

saturation for blindly updating the interaction wrench without considering physical limits of actuators. Therefore, to safely exploit an aerial manipulator in an unstructured, possibly dynamic environment, a pushing strategy should also be aware of such excessive interaction wrench generation.

III. PRELIMINARIES ON SYSTEM ANALYSIS

A. Impulsive switched system

To rigorously analyze a system with both continuous and discontinuous transitions of state variables, we adopt *impulsive switched system* to model a closed-loop system with such hybrid behavior. Let l_d be an index set indicating family of discrete dynamics $\{g_i : i \in l_d\}$, and consider the following impulsive switched system [34–37]:

$$\begin{cases} \dot{x}(t) = f(x(t), \omega(t)), & t \neq t_k, k \in \mathbb{N} \\ x(t^+) = g_{i_k}(x(t^-), \omega(t^-)), & t = t_k, k \in \mathbb{N}, i_k \in l_d \end{cases} \quad (1)$$

where $x \in \mathbb{R}^n$ is the system state, $\omega \in \mathbb{R}^m$ is a locally bounded disturbance input, and \dot{x} denotes the right-hand derivative of x . $x(t^+)$, $x(t^-)$ are defined as $x(t^+) = \lim_{s \rightarrow t^+} x(s)$, $x(t^-) = \lim_{s \rightarrow t^-} x(s)$. If not ambiguous, we use $x^+ := x(t^+)$ and $x^- := x(t^-)$ for brevity. The set of *impulse times* $\{t_k : k \in \mathbb{N}\}$ is a strictly increasing sequence, and we assume non-Zeno behavior as in [34, 35], i.e., discrete dynamics does not occur infinite times in finite time interval [38].

B. Input-to-state stability

Both continuous and discrete dynamics include perturbation terms due to uncertain model parameters and disturbance. To analyze closed-loop system's stability in the presence of such perturbation, one of the widely applied concept is input-to-state stability (ISS) [39]. ISS can be formally defined for the impulsive switched system (1) as follows.

Definition 1 ([36]). *The system (1) is said to be input-to-state stable, if there exist functions $\beta \in \mathcal{KL}$ and $\gamma \in \mathcal{K}_\infty$, such that for each $x_0 \in \mathbb{R}^n$ and input function u , the solution x of (1) exists globally and satisfies*

$$\|x(t)\| \leq \beta(\|x_0\|, t - t_0) + \gamma\left(\sup_{t_0 \leq s \leq t} \|u(s)\|\right). \quad (2)$$

Here, a function $\gamma : [0, \infty) \rightarrow [0, \infty)$ is said to belong to class \mathcal{K} if it is continuous, strictly increasing, and $\gamma(0) = 0$. A function γ belongs to \mathcal{K}_∞ if $\gamma \in \mathcal{K}$ and $\gamma(t) \rightarrow \infty$ as $t \rightarrow \infty$. Furthermore, a function $\beta : [0, \infty) \times [0, \infty) \rightarrow [0, \infty)$ is a class \mathcal{KL} function if $\beta(\cdot, t) \in \mathcal{K}$ for each fixed t , and $\beta(r, t)$ decreases to 0 as $t \rightarrow \infty$ for each fixed r .

C. Average dwell-time

In practice, discrete dynamics incurred by sudden collision or contact-loss does not occur too frequently. To formalize such notion, we introduce a concept of *average dwell-time* (ADT).¹

¹Compared to the concept of *dwell-time* [36] which might not be satisfied during aerial physical interaction due to its hard restriction of positive lower bound to every impulse time interval $t_k - t_{k-1}$, *average dwell-time* is less conservative and can be satisfied in actual experiments since there only exist a finite number of impulses.

Definition 2 ([35, 40]). For each $t \geq \tau \geq 0$, let $N(t, \tau)$ denote the number of impulse times in the open interval (τ, t) . For given $N_0, \tau_D > 0$, and a set of all impulsive signals for which

$$N(t, \tau) \leq N_0 + \frac{t - \tau}{\tau_D}, \quad (3)$$

the constant τ_D is called the average dwell-time and N_0 the chatter bound.

The finite number of impulse condition can be easily transformed to ADT condition by defining N_0 as the upper bound of the number of impulses. Therefore, the idea of average dwell-time can be regarded to be trivially true in actual mechanical systems such as aerial physical interaction, but it is essential in deriving sufficient condition of ISS for impulsive switched system.

D. Lyapunov-based sufficient condition of ISS for impulsive switched system

With a little modification, we derive a Lyapunov-based sufficient condition of ISS for impulsive switched system (1) based on [35] as follows.

Theorem 1. Suppose that there exists a C^1 function $V : \mathbb{R}^n \rightarrow \mathbb{R}$, positive scalars c, d , and three class \mathcal{K}_∞ functions α_1, α_2, χ such that

$$\alpha_1(\|x\|) \leq V(x) \leq \alpha_2(\|x\|) \quad (4a)$$

$$\frac{\partial V}{\partial x} f(x, \omega) \leq -cV(x) + \chi(\|\omega\|) \quad (4b)$$

$$V(g_i(x, \omega)) \leq e^d V(x^-) + \chi(\|\omega\|), \quad \forall i \in l_d \quad (4c)$$

Suppose also that average dwell time (ADT) condition holds with $\tau_D > d/c$ and N_0 arbitrarily. Then the impulsive switched system (1) is input-to-state stable (ISS).

Proof. See appendix A. \square

E. Overview of system modeling, controller design and stability analysis

Although uncertainties and disturbance during continuous dynamics can be compensated through robust control inputs, it is not true during discrete dynamics. This is because impulsive control input at exact timing t_k is required to overcome uncertainties during discrete dynamics, which is typically not available in actual robotic platforms due to difficulty in detecting exact impulse timing and actuating impulsive force/torque. Therefore, instead, we focus on designing a robust controller from which ISS is guaranteed during continuous dynamics and analyze the closed-loop system during discrete dynamics such that ISS of the overall system, which is modeled as an impulsive switched system, is guaranteed. To obtain such result, we first derive an open-loop hybrid system model of aerial physical interaction with a movable object in section IV, and design a disturbance-observer-based robust controller in section V by which ISS during continuous dynamics is guaranteed in Lyapunov sense. Discrete dynamics is then analyzed in section VI where we propose an impulsive switched system

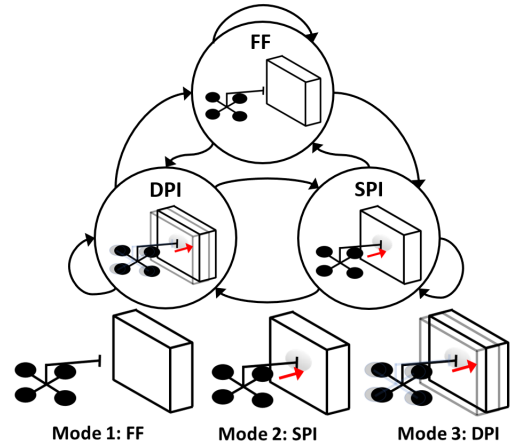


Fig. 2. Hybrid system model of aerial physical interaction with a movable object. Mode 1: FF (Free Flight), Mode 2: SPI (Static Physical Interaction), Mode 3: DPI (Dynamic Physical Interaction).

model for the closed-loop system and analyze ISS property of the impulsive switched system using *Theorem 1*.

The main variables used in system modeling, controller design, and stability analysis can be found in Table I.

F. Notations

Since there appear various systems henceforth, for example, aerial manipulator, underactuated subsystem, fully actuated subsystem, and multirotor, to clarify to which system the variables belong, we uniformly use different subscripts a, u, f, m throughout the paper. For a state variable $x \in \mathbb{R}^n$ and its desired value $x_d \in \mathbb{R}^n$, we define $\tilde{x} = x - x_d$. To express changes in the state x from an impulsive event, x^+ and x^- are used to denote the state after and before the event, respectively. We use $v_i, 0_{j \times k}, \otimes, I_n$, and $\|\cdot\|$ to denote the i^{th} component/row of a vector/matrix v , zero matrix in $\mathbb{R}^{j \times k}$, the Kronecker product, identity matrix in $\mathbb{R}^{n \times n}$, and an induced 2-norm of a matrix. Also, for a column vector a and b , $[a; b] := [a^\top \ b^\top]^\top$. Lastly, c^* , s^* , and t^* denote shorthands for \cos^* , \sin^* , and \tan^* , respectively.

IV. SYSTEM MODELING

We first model an aerial manipulator conducting physical interaction using hybrid system [8] as in Fig. 2. During free-flight, or physical interaction, the system state follows continuous differential equations which can be modeled from Euler-Lagrange equation [5, 19]. A set of these continuous differential equations are called *flow map*. Here, three *modes* are introduced, which are free-flight (*FF*), static physical interaction (*SPI*), and dynamic physical interaction (*DPI*).

Next, we model transition or jump between modes. Impulsive jumps, which are jumps starting from *FF* to any modes, are modeled assuming a rigid body collision [41] since these jumps necessarily include a collision. Instantaneous rebound due to rigid body collision during free-flight is also modeled as an impulsive jump as in [4], namely *FF* to *FF* itself as depicted in Fig. 2. Non-impulsive jumps are also modeled, i.e. jumps starting from *SPI* or *DPI*, to describe a possible

TABLE I
 TABLE OF VARIABLES IN SECTIONS IV, V, VI

Variable	Description
Section IV	
r_c	Center of mass of aerial manipulator
ϕ	ZYX Euler angles of multirotor platform
θ	Joint angles of robotic arm
z_a	Configuration of aerial manipulator $z_a = [r_c; \phi; \theta]$
R	Rotation matrix of multirotor's orientation
T, \hat{T}	Multirotor's total thrust and modified total thrust
τ_ϕ	Multirotor's body torque
τ_θ	Joint torque of robotic arm
Φ	Coupling term between translational and rotational dynamics of multirotor
Φ_d	Φ with ϕ_d instead of ϕ
λ_a	Interaction wrench
δ_a	External disturbance (excluding interaction wrench)
z_u, z_f	Configurations of underactuated, and fully actuated subsystems
u_u, u_f	Control inputs of underactuated, and fully actuated subsystems
δV	End-effector velocity jump
λ_{imp}	Intensity of impulsive interaction wrench
Sections V & VI	
$[z; \dot{z}]$	System state of a general system
Δ	External disturbance of a general system
\tilde{z}	Configuration error between z and z_d
q_i, p_i	Controller states of a general system
u	Control input of a general system
\bar{u}	Nominal control input of a general system
u_{dob}	DOB control input of a general system
ξ_i, η_i	Controller states after coordinate transformation of a general system
ξ_i^*, η_i^*	Quasi-steady state variables of ξ_i, η_i
$\tilde{\xi}_i, \tilde{\eta}_i$	Error variables between ξ_i, η_i and ξ_i^*, η_i^*
y	State error $y = [\tilde{z}; \dot{\tilde{z}}]$ of a general system
x	Concatenated error of a general system $x = [y; \tilde{\eta}]$
f	Dynamics of x
V_1, V_2, V	Quadratic positive-definite functions of $y, \tilde{\eta}$, and x , satisfying $V = V_1 + V_2$
$q_{u,i}, p_{u,i}, q_{f,i}, p_{f,i}$	q_i, p_i of underactuated and fully actuated subsystems
$u_u, \bar{u}_u, u_f, \bar{u}_f$	u, \bar{u} of underactuated and fully actuated subsystems
$u_{u,dob}, u_{f,dob}$	u_{dob} of underactuated and fully actuated subsystems
y_u, y_f, y_m	y of underactuated, fully actuated subsystems, and multirotor system
$\tilde{\eta}_u, \tilde{\eta}_f, \tilde{\eta}_m$	$\tilde{\eta}$ of underactuated, fully actuated subsystems, and multirotor system
x_u, x_f, x_m	x of underactuated, fully actuated subsystems, and multirotor system
f_u, f_f, f_m	Error dynamics of x_u, x_f, x_m
V_u, V_f, V_m	V of underactuated, fully actuated subsystems, and multirotor system
$\delta\lambda$	Interaction wrench jump
$g_{m,i}$	Jump map models ($i = 1, 2, 3$)
$\mathcal{K}_{am}, \mathcal{K}_{ms}$	Kinetic energies of aerial manipulator and movable object

discontinuity of the interaction wrench. For example, these jumps can capture slip in contact during physical interaction. A slip without contact-loss can be represented by jumps from $\{SPI, DPI\}$ to $\{SPI, DPI\}$ while a slip with contact-loss can be modeled by jumps from $\{SPI, DPI\}$ to FF . We use a term *jump map* to describe a set of all possible jumps between modes.

Configuration of an aerial manipulator can be described using $r_c \in \mathbb{R}^3, \phi \in \mathbb{R}^3, \theta \in \mathbb{R}^{n_\theta}$ which denote center of mass (CoM) position of the aerial manipulator, ZYX Euler angles of the multirotor platform, and joint angles of the robotic arm, respectively. Control inputs are the multirotor's total thrust $T \in \mathbb{R}$, the multirotor's body torque $\tau_\phi \in \mathbb{R}^3$, and the joint torque of the robotic arm $\tau_\theta \in \mathbb{R}^{n_\theta}$. However, since most lightweight motors composing a robotic arm equipped on an aerial manipulator are not directly torque-controllable, we do not regard τ_θ as a control input henceforth and instead assume that there exists an exogenous position/velocity controller. To consider underactuatedness of the multirotor and exogenous controller of the robotic arm, we decompose system dynamics of the aerial manipulator in the following subsection as

$$\text{Dynamics} \begin{cases} \text{multirotor} \begin{cases} \text{underactuated subsystem (7a)} \\ \text{fully actuated subsystem (7b)} \end{cases} \\ \text{robotic arm (49)} \end{cases}$$

where derivation of the robotic arm dynamics can be found in appendix B.

A. Flow map

If a model of the interacting dynamic object is known, it would be possible to derive a complete equation of motion of *DPI* mode. However, since physical parameters of the moving object such as mass or moment of inertia are uncertain, and motion constraints of the object due to surrounding environment are also unknown, we model an interaction wrench during *DPI* mode as an external disturbance to the aerial manipulator. Likewise, an interaction wrench during *SPI* mode is also modeled as a disturbance to utilize a single robust controller for all modes. Therefore, equations of motion of *DPI* and *SPI* can be deduced by adding an interaction wrench term to that of *FF* mode.

Using a generalized coordinate $z_a = [r_c; \phi; \theta] \in \mathbb{R}^{6+n_\theta}$, equations of motion of *SPI* and *DPI* modes can be derived from Euler-Lagrange equation as

$$M_a \ddot{z}_a + H_a(z_a, \dot{z}_a) = B_a u_a + J_a^\top \lambda_a + \delta_a \quad (5)$$

where $u_a = [T; \tau_\phi; \tau_\theta]$, $\lambda_a \in \mathbb{R}^6$ is an interaction wrench, $\delta_a \in \mathbb{R}^{n_z}$ is external disturbance except for an interaction wrench. $M_a \in \mathbb{R}^{6+n_\theta \times 6+n_\theta}$, $H_a \in \mathbb{R}^{6+n_\theta}$, $J_a \in \mathbb{R}^{6 \times 6+n_\theta}$ are mass matrix, Coriolis and gravity term, and Jacobian matrix, respectively. We explicitly separate an interaction wrench and external disturbance, and (5) can be easily converted to *FF* mode dynamics by erasing an interaction wrench term $J_a^\top \lambda_a$.

Thanks to [42, Prop. 2], the equations of motion (5) can be decomposed into translational and rotational motions as

$$m_L \ddot{r}_c + m_L g e_3 = Re_3 T + J_r^\top \lambda_a + \delta_r \quad (6a)$$

$$\begin{bmatrix} M_\phi & M_{\phi\theta} \\ M_{\phi\theta}^\top & M_\theta \end{bmatrix} \begin{bmatrix} \ddot{\phi} \\ \ddot{\theta} \end{bmatrix} + \begin{bmatrix} C_\phi \\ C_\theta \end{bmatrix} = \begin{bmatrix} B_\phi \\ B_\theta \end{bmatrix} \begin{bmatrix} \tau_\phi \\ \tau_\theta \end{bmatrix} + \begin{bmatrix} J_\phi^\top \\ J_\theta^\top \end{bmatrix} \lambda_a + \begin{bmatrix} \delta_\phi \\ \delta_\theta \end{bmatrix} \quad (6b)$$

where $m_L, g \in \mathbb{R}$ are the total mass of the aerial manipulator and gravitational acceleration. Note that separation between translational (6a) and rotational (6b) dynamics is possible thanks to the choice of coordinate. Since the robotic arm is assumed to be stabilized by an exogenous controller, we only consider the dynamics of the multirotor. However, dynamic coupling from the motion of the robotic arm to the multirotor is not negligible, and the effect is included in the following modified disturbance term δ_f . To consider underactuatedness of a multirotor, we rearrange (6) to divide equations of motion into an underactuated part $z_u = [r_{c,1}; r_{c,2}] \in \mathbb{R}^2$ and a fully actuated part $z_f = [r_{c,3}; \phi] \in \mathbb{R}^4$ as

$$m_L \ddot{z}_u = \Psi \Phi_d \hat{T} + J_u^\top \lambda_a + \delta_u \quad (7a)$$

$$M_f \ddot{z}_f + C_f = B_f \begin{bmatrix} \hat{T} \\ \tau_\phi \end{bmatrix} + J_f^\top \lambda_a + \delta_f \quad (7b)$$

where $\hat{T} = e_3^\top Re_3 T$, $\delta_u = \Psi(\Phi - \Phi_d) \hat{T} + [\delta_{r,1}; \delta_{r,2}]$, $\delta_f = [\delta_{r,3}; \delta_\phi - M_{\phi\theta} \ddot{\theta}]$,

$$M_f = \begin{bmatrix} m_L & 0 \\ 0 & M_\phi \end{bmatrix}, C_f = \begin{bmatrix} m_L g \\ C_\phi \end{bmatrix}, B_f = \begin{bmatrix} 1 & 0 \\ \hat{S}_\phi^\top Re_3 & Q^\top \end{bmatrix},$$

and $\hat{S}_\phi = S_\phi / (e_3^\top Re_3) \in \mathbb{R}^{3 \times 3}$.² $J_u = [J_r e_1 \ J_r e_2]$ and $J_f = [J_r e_3 \ J_\phi]$. Ψ and Φ are defined as

$$\Psi = \begin{bmatrix} c\phi_3 & s\phi_3 \\ s\phi_3 & -c\phi_3 \end{bmatrix}, \Phi = \begin{bmatrix} t\phi_2 \\ t\phi_1/c\phi_2 \end{bmatrix},$$

and from definition, $\Psi \Phi \hat{T} = [I_2 \ 0_{2 \times 1}] Re_3 T$. By inverting the mass matrices in (7), equations of motion can be written as

$$\ddot{z}_u = G_u u_u + \Delta_u \quad (8a)$$

$$\ddot{z}_f = F_f + G_f u_f + \Delta_f \quad (8b)$$

where $G_u = m_L^{-1} \Psi \hat{T}$, $\Delta_u = m_L^{-1} (J_u^\top \lambda_a + \delta_u)$, $F_f = -M_f^{-1} C_f$, $G_f = M_f^{-1} B_f$, $\Delta_f = M_f^{-1} (J_f^\top \lambda_a + \delta_f)$, $u_u = \Phi_d$, and $u_f = [\hat{T}, \tau_\phi]^\top$. Note that the effect of discontinuity in Δ_u, Δ_f on stability, which is induced by discontinuity in the interaction wrench λ_a , will be analyzed in section VI.

Remark 1. To handle underactuatedness of a conventional multirotor, desired roll, pitch angles $\phi_{1,d}, \phi_{2,d}$ should be calculated from a control input of the underactuated subsystem. Our previous work [5] and other existing works [30, 43] rely on $\arcsin(\cdot)$ to solve this problem, but due to the limited domain $[-1, 1] \in \mathbb{R}$, the problem can become ill-posed especially in applying robust controllers since they often generate large-amplitude control inputs to compensate disturbance. To address this problem, similar to [44, 45], we formulate the control input for the underactuated subsystem $u_u = \Phi_d$

²A definition of S_ϕ can be found in appendix C.

using only $\tan(\cdot)$, and thus, the inversion problem from Φ_d to $\phi_{1,d}, \phi_{2,d}$ becomes feasible for every $u_u = \Phi_d \in \mathbb{R}^2$.

B. Jump map

Jumps can be classified into impulsive and non-impulsive jumps. We model impulsive jumps based on rigid body collision assumption applied in various robot-environment interaction tasks [3, 4].

1) *Impulsive jump*: Every jump from *FF* mode can be interpreted with an impulsive jump. By assuming that a generalized position z does not change during the impact, and control input u and disturbance δ do not contain impulses, the following equation of generalized momentum conservation can be obtained by "integrating" (5) over the "duration" of the impact as [3]

$$M_a (\dot{z}_a^+ - \dot{z}_a^-) = J_a^\top \lambda_{imp}. \quad (9)$$

where $(*)^+, (*)^-$ denote values of $(*)$ just after and before the impact, and $\lambda_{imp} = \int_{t^-}^{t^+} \lambda_a(\tau) d\tau$ is the intensity of the impulsive interaction wrench.

In [3], perfectly plastic impact and static contact surface are further assumed so that an impact model is written as

$$J_a \dot{z}_a^+ = 0.$$

However, for aerial physical interaction with a possibly dynamic object, imperfect elastic impact and motion of a contact surface should be considered. Therefore, we modify the impact model at a contact point/surface (or an end-effector of the robotic arm) as

$$J_a (\dot{z}_a^+ - \dot{z}_a^-) = \delta V \quad (10)$$

where $\delta V \in \mathbb{R}^6$ denotes a change in the end-effector twist before and after the impact. For perfectly plastic collision, $\delta V = -J_a \dot{z}_a^- + \mathcal{V}_s^+$ where $\mathcal{V}_s^+ \in \mathbb{R}^6$ describes the movable object's twist at the contact surface. Since there exists no universal law for modeling δV [41], and most models require physical parameters of the contact surface including static/dynamic friction coefficient and coefficient of restitution, we leave the term unmodeled. Note that the term δV will be considered as perturbation to the system and analyzed in the stability analysis of the entire impulsive switched system.

Combining (9) and (10), the overall impact model can be written as

$$\begin{bmatrix} M_a & -J_a^\top \\ J_a & 0 \end{bmatrix} \begin{bmatrix} \dot{z}_a^+ \\ \lambda_{imp} \end{bmatrix} = \begin{bmatrix} M_a \dot{z}_a^- \\ J_a \dot{z}_a^- + \delta V \end{bmatrix} \quad (11)$$

from which the closed-form solution can be obtained as

$$\dot{z}_a^+ = \dot{z}_a^- + J_a^\dagger \delta V, \quad \lambda_{imp} = (J_a M_a^{-1} J_a^\top)^{-1} \delta V \quad (12)$$

where $J_a^\dagger := M_a^{-1} J_a^\top (J_a M_a^{-1} J_a^\top)^{-1}$ is a weighted pseudo-inverse of J_a with weight M_a .

2) *Non-impulsive jump*: Unlike jumps starting from *FF* mode, every jump from *SPI* or *DPI* is non-impulsive. Therefore, there exists no change in the system state during the jumps. However, discontinuity in the interaction wrench can occur because taking *DPI* \rightarrow *FF* as an example, interaction wrench vanishes during the jump. Such discontinuity

in interaction wrench will be further discussed in the jump map analysis. The state change during non-impulsive jump is modeled as

$$z_a^+ = z_a^-, \quad \dot{z}_a^+ = \dot{z}_a^-. \quad (13)$$

V. CONTROLLER DESIGN AND FLOW MAP ANALYSIS

In this section, we design a robust controller based on disturbance-observer (DOB) [46] that not only guarantees input-to-state stability but also arbitrarily minimizes the effect of disturbance. It will be shown that theoretically, the effect of disturbance can be made to be arbitrarily small by modulating a control parameter ϵ . Variables with no subscript are used when describing system dynamics and controller for a general nonlinear system to distinguish variables from those for the aerial manipulator.

Although the proposed robust controller shares similar structure to those in [5, 30], they only analyze transient performance with respect to nominal dynamics. In contrast, to facilitate stability analysis of each mode and also the overall hybrid system, we additionally 1) augment the control structure to include nominal control input \bar{u} , 2) analyze further to show ISS stability of the closed-loop system of each mode, and 3) prove disturbance attenuation in the closed-loop system perspective.

A. DOB-based controller design for generalized nonlinear system

Since every subsystem of the system dynamics of each mode (8a), (8b) has the same form as (14), we first design a controller for the below generalized nonlinear system:

$$\dot{z} = F(z, \dot{z}, t) + G(z, \dot{z}, t)u + \Delta \quad (14)$$

where $[z; \dot{z}] \in \mathbb{R}^{2n_z}$ is a system state, $u \in \mathbb{R}^{n_u}$ is a control input, and Δ is an external disturbance. To consider parametric uncertainties, we write nominal counterparts of $F(z, \dot{z}, t)$ and $G(z, \dot{z}, t)$ as $\bar{F}(z, \dot{z}, t)$ and $\bar{G}(z, \dot{z}, t)$. Nominal dynamics can be constructed using nominal parameters of a system, or even a different structure can be utilized [30]. Thanks to the full actuation assumption, $n_u = n_z$ and $G, \bar{G} \in \mathbb{R}^{n_z \times n_z}$ are invertible.

A DOB-based controller is designed as follows:

$$\dot{q}_i = Aq_i + Bz_i, \quad \dot{p}_i = Ap_i + B\bar{G}_i u, \quad (15a)$$

$$u = \bar{u} + \bar{G}^{-1}u_{dob}, \quad u_{dob,i} = p_{i,1} - (\dot{q}_{i,2} - \bar{F}_i), \quad (15b)$$

$$\bar{u} = \bar{G}^{-1}(\ddot{z}_d - K_p \ddot{z} - K_d \dot{\ddot{z}} - \bar{F}) \quad (15b)$$

where $p_i, q_i \in \mathbb{R}^2$ are controller states with $i = 1, \dots, n_z$, and

$$A = \begin{bmatrix} 0 & 1 \\ -a_0/\epsilon^2 & -a_1/\epsilon \end{bmatrix}, \quad B = \begin{bmatrix} 0 \\ a_0/\epsilon^2 \end{bmatrix},$$

with $a_0, a_1 > 0$ being tuning parameters and $\epsilon > 0$ being an arbitrarily small constant. $K_p, K_d \in \mathbb{R}^{n_z \times n_z}$ in (15b) are positive definite control gain matrices.

To analyze disturbance attenuation property, we conduct the following coordinate transformation for p_i, q_i :

$$\xi_i = \begin{bmatrix} \frac{1}{\epsilon} q_{i,1} + \frac{a_1}{a_0} q_{i,2} - \frac{1}{\epsilon} z_i \\ q_{i,2} - \dot{z}_i \end{bmatrix}, \quad \eta_i = \begin{bmatrix} p_{i,1} - \dot{q}_{i,2} \\ \epsilon(\dot{p}_{i,1} - \ddot{q}_{i,2}) \end{bmatrix}. \quad (16)$$

From (15a) and (16), dynamics of ξ_i and η_i can be obtained as

$$\epsilon \dot{\xi}_i = A_\xi \xi_i - \epsilon E_2 (F_i + G_i u + \Delta_i) \quad (17a)$$

$$\epsilon \dot{\eta}_i = A_\eta \eta_i + a_0 E_2 (\bar{G}_i u - (F_i + G_i u + \Delta_i)) \quad (17b)$$

where $E_2 = [0; 1]$, and

$$A_\xi = \begin{bmatrix} -a_1 & 1 \\ -a_0 & 0 \end{bmatrix}, \quad A_\eta = \begin{bmatrix} 0 & 1 \\ -a_0 & -a_1 \end{bmatrix}.$$

From the singular perturbation theory [47, Ch. 11], by taking $\epsilon = 0$, the quasi-steady state ξ^*, η^* can be derived from (17) as $\xi_i^* = 0, \eta_{i,2}^* = 0$, and

$$\eta_{i,1}^* = \bar{G}_i u^* - (F_i + G_i u^* + \Delta_i). \quad (18)$$

Defining error variables as $\tilde{\xi}_i = \xi_i - \xi_i^*, \tilde{\eta}_i = \eta_i - \eta_i^*$, error dynamics are derived as

$$\epsilon \dot{\tilde{\xi}}_i = A_\xi \tilde{\xi}_i - \epsilon E_2 (F_i + G_i u + \Delta_i) \quad (19a)$$

$$\epsilon \dot{\tilde{\eta}}_i = A_\eta \tilde{\eta}_i + \epsilon \dot{\eta}_i^*. \quad (19b)$$

Defining $\eta_{[1]} = [\eta_{1,1}; \dots; \eta_{n_z,1}] \in \mathbb{R}^{n_z}$, using (15a), (18), and the fact that $u_{dob} = \eta_{[1]} + \bar{F}$,

$$\eta_{[1]}^* = \bar{G} G^{-1} \{ (\bar{G} - G) \bar{u} + (\bar{F} - F) - G \bar{G}^{-1} \bar{F} - \Delta \}. \quad (20)$$

Therefore, applying (15a) and (20) to (14),

$$\ddot{z} = \bar{F} + \bar{G} \bar{u} + G \bar{G}^{-1} \tilde{\eta}_{[1]}. \quad (21)$$

Now, combining (21) and (15b), the closed-loop system can be written with $y = [\ddot{z}; \dot{\tilde{z}}]$ as

$$\dot{y} = A_y y + (E_2 \otimes I_{n_z}) G \bar{G}^{-1} (I_{n_z} \otimes E_1^\top) \tilde{\eta} \quad (22a)$$

$$\dot{\tilde{\eta}} = \frac{1}{\epsilon} (I_{n_z} \otimes A_\eta) \tilde{\eta} + \dot{\eta}^* \quad (22b)$$

where $E_1 = [1; 0]$, $\tilde{\eta} = [\tilde{\eta}_1; \dots; \tilde{\eta}_{n_z}]$ and

$$A_y = \begin{bmatrix} 0_{n_z \times n_z} & I_{n_z} \\ -K_p & -K_d \end{bmatrix}.$$

Note that we omit $\tilde{\xi}$ in the closed-loop system analysis since it has no effect on the time evolution of y . However, boundedness of $\tilde{\xi}$ can still be shown and refer to [46] for such analysis.

Now, we propose the following:

Proposition 1. Consider Lyapunov candidates

$$V_1(y) = \frac{1}{2} y^\top P_y y \quad (23a)$$

$$V_2(\tilde{\eta}) = \frac{1}{2} \tilde{\eta}^\top P_\eta \tilde{\eta} \quad (23b)$$

where $P_y \in \mathbb{R}^{2n_z \times 2n_z}, P_\eta \in \mathbb{R}^{n_z \times n_z}$ are symmetric, positive-definite matrices satisfying $P_y A_y + A_y^\top P_y = -2I_{2n_z}, P_\eta (I_{n_z} \otimes A_\eta) + (I_{n_z} \otimes A_\eta)^\top P_\eta = -2I_{n_z}$. Then, for a Lyapunov function

$$V(y, \tilde{\eta}) = V_1(y) + V_2(\tilde{\eta}), \quad (24)$$

there exist a positive constant c and a class \mathcal{K}_∞ function χ satisfying

$$\dot{V} = \frac{\partial V}{\partial x} f(x, \dot{x}) \leq -cV + \chi(\|\sqrt{\epsilon} \dot{\eta}^*\|) \quad (25)$$

where $x = [y; \tilde{\eta}]$, $\dot{x} = f(x, \dot{\eta}^*)$ is defined from (22).

Proof. Since A_y, A_η are Hurwitz, such P_y, P_η exist. Taking time derivatives of V ,

$$\begin{aligned} \dot{V} &\leq -\|y\|^2 - \frac{1}{\epsilon} \|\tilde{\eta}\|^2 + \|P_\eta\| \|\dot{\eta}^*\| \|\tilde{\eta}\| \\ &\quad + \|G\bar{G}^{-1}\| \|P_y\| \|y\| \|\tilde{\eta}\|. \end{aligned}$$

From the Young's inequality, there exist constants $\alpha, \beta > 0$ satisfying $\|y\| \|\tilde{\eta}\| \leq \alpha \|y\|^2 + \frac{1}{4\alpha} \|\tilde{\eta}\|^2$, $\|\dot{\eta}^*\| \|\tilde{\eta}\| \leq \beta \epsilon \|\dot{\eta}^*\|^2 + \frac{1}{4\beta\epsilon} \|\tilde{\eta}\|^2$. Therefore, the following holds

$$\dot{V} \leq -b_1 \|y\|^2 - b_2(\epsilon) \|\tilde{\eta}\|^2 + \beta \|P_\eta\| \|\sqrt{\epsilon} \dot{\eta}^*\|^2$$

where $b_1 := 1 - \alpha \|G\bar{G}^{-1}\| \|P_y\|$, $b_2(\epsilon) := \frac{1}{\epsilon} - \frac{\|G\bar{G}^{-1}\| \|P_y\|}{4\alpha} - \frac{\|P_\eta\|}{4\beta\epsilon}$. Since $\epsilon > 0$ can be taken to be arbitrarily small, there exist $\alpha, \beta, \epsilon > 0$ satisfying $b_1, b_2(\epsilon) > 0$.³ Therefore, from the quadratic property of V , the following holds

$$\dot{V} \leq -cV + \chi(\|\sqrt{\epsilon} \dot{\eta}^*\|)$$

with $c = \min\{2b_1/\|P_y\|, 2b_2(\epsilon)/\|P_\eta\|\}$, $\chi(r) = \beta \|P_\eta\| r^2$. \square

As can be seen in (20), $\dot{\eta}^*$ contains both model uncertainties and external disturbances. However, since ϵ can be taken to be arbitrarily small, the perturbing effect of model uncertainties and external disturbances can be mitigated by taking sufficiently small ϵ .

B. Application to aerial manipulator

We separate the aerial manipulator's dynamics of each mode into the multirotor's fully actuated subsystem, underactuated subsystem, and the robotic arm. Since we deploy an exogenous controller for the robotic arm, we only consider controller design for the multirotor part. The proposed DOB-based controller can be applied to both subsystems of a multirotor because both subsystems share the form of (14).

Since all three *FF*, *SPI*, *DPI* modes are modeled to have the same structure as in (8), a common DOB-based controller is designed, which operates regardless of mode change. For the underactuated subsystem (8a), the controller is designed as

$$\begin{aligned} \dot{q}_{u,i} &= A_u q_{u,i} + B_u z_{u,i}, & \dot{p}_{u,i} &= A_u p_{u,i} + B_u \bar{G}_{u,i} u_u, \\ u_u &= \bar{u}_u + \bar{G}_u^{-1} u_{u,dob}, & u_{u,dob} &= p_{u,[1]} - \dot{q}_{u,[2]}, \\ \bar{u}_u &= \bar{G}_u^{-1} (\ddot{z}_{u,d} - K_{up} \dot{z}_u - K_{ud} \dot{z}_u) \end{aligned} \quad (26)$$

and for the fully actuated subsystem (8b),

$$\begin{aligned} \dot{q}_{f,i} &= A_f q_{f,i} + B_f z_{f,i}, & \dot{p}_{f,i} &= A_f p_{f,i} + B_f \bar{G}_{f,i} u_f, \\ u_f &= \bar{u}_f + \bar{G}_f^{-1} u_{f,dob}, & u_{f,dob} &= p_{f,[1]} - (\dot{q}_{f,[2]} - \bar{F}_f), \\ \bar{u}_f &= \bar{G}_f^{-1} (\ddot{z}_{f,d} - K_{fp} \dot{z}_f - K_{fd} \dot{z}_f - \bar{F}_f). \end{aligned} \quad (27)$$

For brevity, we use a notation $*_{[1]} := [*_{1,1}; \dots; *_{n,1}] \in \mathbb{R}^n$, $*_{[2]} := [*_{1,2}; \dots; *_{n,2}] \in \mathbb{R}^n$ where $* = [*_1; \dots; *_{n,1}] \in \mathbb{R}^{nm}$, $*_i \in \mathbb{R}^m \forall i = 1, \dots, n$. Newly defined controller states are $p_u, q_u \in \mathbb{R}^4$ for the underactuated subsystem and $p_f, q_f \in \mathbb{R}^8$ for the fully-actuated subsystem. A_u, B_u, A_f, B_f inherit the

³Take $\alpha < \frac{\|P_y\|}{\|G\bar{G}^{-1}\|}$, $\beta > \frac{\|P_\eta\|}{4}$, and $\epsilon < \frac{4\alpha}{\|G\bar{G}^{-1}\| \|P_y\|} \left(1 - \frac{\|P_\eta\|}{4\beta}\right)$.

structure of A, B defined in subsection V-A, and $\bar{G}_u, \bar{G}_f, \bar{F}_f$ are defined to have the same structure as G_u, G_f, F_f but with nominal parameters.

Lemma 1. *Let $x_m = [x_u; x_f]$ and $\dot{\eta}_m^* = [\dot{\eta}_u^*; \dot{\eta}_f^*]$. Then, for the closed-loop system of the multirotor part $\dot{x}_m = f_m(x_m, \dot{\eta}_m^*)$ which can be obtained from (8), (26), and (27), there exist a common Lyapunov function V_m , a positive constant c_m , and a class \mathcal{K}_∞ function χ_m^c satisfying*

$$\dot{V}_m = \frac{\partial V_m}{\partial x_m} f_m(x_m, \dot{\eta}_m^*) \leq -c_m V_m + \chi_m^c(\|\sqrt{\epsilon_m} \dot{\eta}_m^*\|) \quad (28)$$

with arbitrarily small positive constant $\epsilon_m := \max\{\epsilon_u, \epsilon_f\}$ where ϵ_u, ϵ_f are control parameter ϵ for underactuated and fully actuated subsystems.

Proof. For both the underactuated and fully actuated subsystems, the following closed-loop systems can be obtained using (8), (26), and (27) as

$$\begin{aligned} \dot{x}_u &= f_u(x_u, \dot{\eta}_u^*) \\ \dot{x}_f &= f_f(x_f, \dot{\eta}_f^*) \end{aligned}$$

which are defined similarly as $f(x, \dot{\eta}^*)$ in Proposition 1. Then, thanks to Proposition 1, there exist Lyapunov functions for the underactuated and fully actuated subsystems

$$\begin{aligned} V_u(y_u, \tilde{\eta}_u) &= V_{u,1}(y_u) + V_{u,2}(\tilde{\eta}_u), \\ V_f(y_f, \tilde{\eta}_f) &= V_{f,1}(y_f) + V_{f,2}(\tilde{\eta}_f) \end{aligned} \quad (29)$$

each satisfying (25) as

$$\begin{aligned} \dot{V}_u &= \frac{\partial V_u}{\partial x_u} f_u(x_u, \dot{\eta}_u^*) \leq -c_u V_u + \chi_u(\|\sqrt{\epsilon_u} \dot{\eta}_u^*\|), \\ \dot{V}_f &= \frac{\partial V_f}{\partial x_f} f_f(x_f, \dot{\eta}_f^*) \leq -c_f V_f + \chi_f(\|\sqrt{\epsilon_f} \dot{\eta}_f^*\|) \end{aligned} \quad (30)$$

where $c_u, c_f > 0$, $\chi_u, \chi_f \in \mathcal{K}_\infty$. Thus, by constructing a common Lyapunov function $V_m = V_u + V_f$ for all three modes, and with a definition of $f_m(x_m, \dot{\eta}_m^*) = [f_u(x_u, \dot{\eta}_u^*); f_f(x_f, \dot{\eta}_f^*)]$, we can conclude (28) with $c_m = \min\{c_u, c_f\} > 0$, $\chi_m^c(x) = 2 \max\{\chi_u(x), \chi_f(x)\} \in \mathcal{K}_\infty$, $\dot{\eta}_m^* = [\dot{\eta}_u^*; \dot{\eta}_f^*]$, and $\epsilon_m = \max\{\epsilon_u, \epsilon_f\}$. \square

VI. JUMP MAP ANALYSIS AND ANALYSIS OF OVERALL IMPULSIVE SWITCHED SYSTEM

To guarantee stability of an aerial manipulator even in the presence of sudden contact-loss or collision during interaction with a possibly dynamic object, we show that jumps by contact-loss and collision satisfy ISS property with respect to perturbation by end-effector velocity jump δV and interaction wrench jump $\delta \lambda$. Then, with an additional mild assumption of kinetic energy increase of the movable object after a collision, less conservative results are derived where end-effector velocity jump δV is no longer considered as perturbation.

For the ease of notation, we define $V_m(y_m, \tilde{\eta}_m) = V_{m,1}(y_m) + V_{m,2}(\tilde{\eta}_m)$ where

$$\begin{aligned} V_{m,1}(y_m) &= V_{u,1}(y_u) + V_{f,1}(y_f), \\ V_{m,2}(\tilde{\eta}_m) &= V_{u,2}(\tilde{\eta}_u) + V_{f,2}(\tilde{\eta}_f), \end{aligned}$$

and $y_m = [y_u; y_f]$, $\tilde{\eta}_m = [\tilde{\eta}_u; \tilde{\eta}_f]$. In the following analysis, we use the fact that the reference state does not change during jumps, i.e.

$$z_{m,d}^+ = z_{m,d}^-, \quad \dot{z}_{m,d}^+ = \dot{z}_{m,d}^- \quad (31)$$

A. System state jump

From (31), (12), and the fact that $y_m = [\tilde{z}_u; \dot{\tilde{z}}_u; \tilde{z}_f; \dot{\tilde{z}}_f]$,

$$y_m^+ = y_m^- + E_m J_a^\dagger \delta V \quad (32)$$

where $E_m = [0_{2 \times (6+n_\theta)}; E_u; 0_{4 \times (6+n_\theta)}; E_f]$, $E_u = [I_2 \ 0_{2 \times (4+n_\theta)}]$, $E_f = [0_{4 \times 2} \ I_4 \ 0_{4 \times n_\theta}]$. Therefore, there exist positive constants $c_{m,0} > 1, c_{m,1}$ satisfying

$$|V_{m,1}(y_m^+) - V_{m,1}(y_m^-)| \leq c_{m,0} V_{m,1}(y_m^-) + c_{m,1} \|\delta V\|^2 \quad (33)$$

where quadratic property, positive-definiteness of $V_{m,1}(y_m)$, and upper-boundedness of $\|J_a^\dagger\|$ are used.

B. Controller state jump

To investigate controller state jump, we first need to derive what $\tilde{\eta}^+ - \tilde{\eta}^-$ is. Since there exist multiple controller states, i.e. $\tilde{\eta}_u, \tilde{\eta}_f$, we first consider a general form appeared in subsection V-A for brevity. Consider a generalized nonlinear system (14), but with Δ replaced by $M^{-1}(J^\top \lambda + \delta)$ as

$$\ddot{z} = F(z, \dot{z}, t) + G(z, \dot{z}, t)u + M^{-1}(J^\top \lambda + \delta).$$

We distinguish the interaction wrench $J^\top \lambda$ from other disturbances δ in Δ to examine discontinuity in interaction wrench. By utilizing (15a) and (16), $\tilde{\eta}$ can be rewritten as

$$\begin{aligned} \tilde{\eta}_{[1]} &= p_{[1]} + \frac{a_0}{\epsilon} \left(\frac{1}{\epsilon} (q_{[1]} - z) + \frac{a_1}{a_0} q_{[2]} \right) - \eta_{[1]}^* \\ \tilde{\eta}_{[2]} &= \epsilon p_{[2]} - \frac{a_0 a_1}{\epsilon^2} (q_{[1]} - z) + \frac{1}{\epsilon} ((a_0 - a_1^2) q_{[2]} - a_0 \dot{z}). \end{aligned}$$

According to (15a), p, q do not jump during jumps. Therefore, $\eta_{[1]}^+ = \eta_{[1]}^-$ can be obtained from (15a) and (16). Then, $\tilde{\eta}^+ - \tilde{\eta}^-$ can be computed as

$$\begin{aligned} \tilde{\eta}_{[1]}^+ - \tilde{\eta}_{[1]}^- &= (\tilde{G} - I_{n_z}) K_d (\dot{z}^+ - \dot{z}^-) + \tilde{G} M^{-1} J^\top (\lambda^+ - \lambda^-) \\ \tilde{\eta}_{[2]}^+ - \tilde{\eta}_{[2]}^- &= -\frac{a_0}{\epsilon} (\dot{z}^+ - \dot{z}^-) \end{aligned} \quad (34)$$

where $\tilde{G} = \tilde{G} G^{-1}$, and the definition of $\eta_{[1]}^*$ can be found in (20) with $\Delta = M^{-1}(J^\top \lambda + \delta)$. Since we are interested in analyzing $\tilde{\eta}_u$ and $\tilde{\eta}_f$, we need to replace z with z_u and z_f . Since $z_u = E_u z_a$ and $z_f = E_f z_a$, for generalization purpose, we use the matrix E to denote $z = E z_a$. Then, $\dot{z}^+ - \dot{z}^-$ in (34) can be written as $E(\dot{z}_a^+ - \dot{z}_a^-)$. Combining (34) with (12) and using the fact that $\tilde{\eta} = (I_{n_z} \otimes E_1) \tilde{\eta}_{[1]} + (I_{n_z} \otimes E_2) \tilde{\eta}_{[2]}$,

$$\tilde{\eta}^+ - \tilde{\eta}^- = C_1 \delta V + C_2 \delta \lambda \quad (35)$$

where $\delta \lambda = \lambda^+ - \lambda^-$, and

$$\begin{aligned} C_1 &= \left\{ (I_{n_z} \otimes E_1) (\tilde{G} - I_{n_z}) K_d - \frac{a_0}{\epsilon} (I_{n_z} \otimes E_2) \right\} E J_a^\dagger, \\ C_2 &= (I_{n_z} \otimes E_1) \tilde{G} M^{-1} J^\top. \end{aligned}$$

Therefore, by concatenating (35) for $\tilde{\eta}_u$ and $\tilde{\eta}_f$,

$$\tilde{\eta}_m^+ = \tilde{\eta}_m^- + C_{m,1} \delta V + C_{m,2} \delta \lambda \quad (36)$$

where $C_{m,1}, C_{m,2}$ are defined as C_1, C_2 but with parameters of multi-rotor closed-loop dynamics.

Now, by applying quadratic property, positive-definiteness of $V_{m,2}(\tilde{\eta}_m)$, and upper-boundedness of $\|C_{m,1}\|$ and $\|C_{m,2}\|$, there exist $d_{m,0} > 1, d_{m,1}, d_{m,2} > 0$ satisfying

$$V_{m,2}(\tilde{\eta}_m^+) \leq d_{m,0} V_{m,2}(\tilde{\eta}_m^-) + d_{m,1} \|\delta V\|^2 + d_{m,2} \|\delta \lambda\|^2. \quad (37)$$

Lemma 2. *There exist a positive constant d_m and $\chi_m^d \in \mathcal{K}_\infty$ satisfying*

$$V_m(x_m^+) \leq e^{d_m} V_m(x_m^-) + \chi_m^d (\|\delta V; \delta \lambda\|). \quad (38)$$

Proof. Since $V_m(x_m) = V_{m,1}(y_m) + V_{m,2}(\tilde{\eta})$, (38) can be achieved by combining (33) and (37). \square

Therefore, every jump in the hybrid system model in Fig. 1 satisfies (38). Particularly, jumps without end-effector velocity jump such as $\{SPI, DPI\} \rightarrow \{SPI, DPI\}$ and $\{SPI, DPI\} \rightarrow FF$ satisfy

$$V_m(x_m^+) \leq e^{d_m} V_m(x_m^-) + \chi_m^d (\|\delta \lambda\|),$$

and jumps without interaction wrench jump, for example $FF \rightarrow FF$, satisfy

$$V_m(x_m^+) \leq e^{d_m} V_m(x_m^-) + \chi_m^d (\|\delta V\|),$$

and other jumps including $FF \rightarrow \{SPI, DPI\}$ satisfy (38).

C. Stability analysis of the entire impulsive switched system

Before providing the final stability result, we derive the closed-loop impulsive switched system model for aerial physical interaction with a movable object as

$$\dot{x}_m = f_m(x_m, \eta_m^*) \quad t \neq t_k, \quad k \in \mathbb{N} \quad (39a)$$

$$x_m^+ = g_{m,i_k}(x_m, \delta V, \delta \lambda) \quad t = t_k, \quad k \in \mathbb{N}, \quad i_k \in l_d \quad (39b)$$

where $f_m(x_m, \eta_m^*)$ is defined in Lemma 1, $l_d = \{1, 2, 3\}$, and

$$\begin{aligned} g_{m,1}(x_m^-, \delta V, \delta \lambda) &:= \begin{bmatrix} y_m^- + E_m J_a^\dagger \delta V \\ \tilde{\eta}_m^- + C_{m,1} \delta V + C_{m,2} \delta \lambda \end{bmatrix}, \\ g_{m,2}(x_m^-, \delta V, \delta \lambda) &:= \begin{bmatrix} y_m^- + E_m J_a^\dagger \delta V \\ \tilde{\eta}_m^- + C_{m,1} \delta V \end{bmatrix}, \\ g_{m,3}(x_m^-, \delta V, \delta \lambda) &:= \begin{bmatrix} y_m^- \\ \tilde{\eta}_m^- + C_{m,2} \delta \lambda \end{bmatrix}. \end{aligned}$$

The flow map model (39a) defined in Lemma 1 is obtained by concatenating closed-loop systems (22) of underactuated and fully actuated parts, and the jump map model (39b) is derived from (32) and (36). The first two jump map models $g_{m,1}, g_{m,2}$ represent impulsive jump, $FF \rightarrow \{SPI, DPI\}$ and $FF \rightarrow FF$ respectively, and the last jump model $g_{m,3}$ is for non-impulsive jump $\{SPI, DPI\} \rightarrow FF$, $\{SPI, DPI\} \rightarrow \{SPI, DPI\}$. Although we know that only one model among $g_{m,1}, g_{m,2}$, and $g_{m,3}$ is activated at a single instant (i.e. they cannot be activated simultaneously), it is unpredictable which jump model is triggered at every impulse time t_k . We model such phenomenon using an impulse signal $\{t_k, i_k\}$. $i_k \in l_d$ is a piecewise constant signal indicating the activated jump model among $g_{m,1}, g_{m,2}$, and $g_{m,3}$, and in definition, it is not defined in advance to express every possible type of jumps.

Now, we present the main result which formally guarantees robust stability of aerial physical interaction with a movable object in the presence of 1) model uncertainty and sufficiently smooth external disturbance, 2) velocity jump modeling collision and 3) interaction wrench jump that models contact-loss and slip in contact.

Theorem 2. Define $\omega = [\sqrt{\epsilon_m} \dot{q}_m^*; \delta V; \delta \lambda]$. Then, the closed-loop impulsive switched system (39) can be written as

$$\begin{cases} \dot{x}_m = f_m(x_m, \omega), & t \neq t_k, k \in \mathbb{N} \\ x_m^+ = g_{m, i_k}(x_m, \omega), & t = t_k, k \in \mathbb{N}, i_k \in l_d \end{cases} \quad (40)$$

Then, the system (40) is uniformly ISS to ω if ADT condition holds with τ_D, N_0 satisfying the premise of Theorem 1.

Proof. The proof is finished with Theorem 1, Lemma 1 and Lemma 2. \square

Remark 2. By definition, the impulsive switched system model (40) allows arbitrary impulse time sequence $\{t_k\}$ and arbitrary impulsive signal $\{i_k\}$ between jump map. Therefore, by analyzing stability of the system (40), we could guarantee stability during the whole operation of aerial physical interaction even in the presence of sudden, unintentional collision or contact-loss with an object without assuming any knowledge of impact timing or impact model.

Thanks to Theorem 1 and the fact that only a finite number of jumps occur during aerial physical interaction, the multirotor part is guaranteed to be ISS throughout the whole interaction with a movable object. This is because N_0 can be taken as the upper bound of the number of jumps and τ_D as an arbitrary constant satisfying $\tau_D > d/c$ as in Theorem 1. Note that this guarantees ultimate boundedness of the state error of the multirotor part even if the aerial manipulator undergoes multiple (but finite) times of detachment and collision with a movable object given that such perturbation are bounded. This certainly goes beyond the result in [5] where ultimate boundedness of the state error is only guaranteed under the condition that disturbance is at least \mathcal{C}^2 .

D. Nominal jump condition

From Theorem 2, ISS property and ultimate boundedness are guaranteed during the aerial physical interaction. However, if the two conditions below hold, we can remove one type of perturbation, which allows less conservative result in the sense of a smaller error bound. We show that, contrary to the original setup involving both δV and $\delta \lambda$ as perturbation terms, δV is no longer perturbation during jumps under such conditions.

In that regard, we call the following the nominal conditions:

- Kinetic energy of the movable object increases after collision,
- Desired velocity of the end-effector is 0 just prior to jumps.

Since the objective of aerial physical interaction in the paper is to move a possibly dynamic object, it can be expected that most collisions, intended or not, result in velocity increase of the movable object. Therefore, in most cases, the first condition is satisfied. The second condition can be imposed

to the planning module, and accordingly, it is automatically satisfied.

Denoting kinetic energy of the aerial manipulator as \mathcal{K}_{am} and that of the movable object as \mathcal{K}_{ms} , the kinetic energy loss of the entire system including the aerial manipulator and the movable object after the impact [41] can be written as

$$\mathcal{K}_{am}^+ + \mathcal{K}_{ms}^+ < \mathcal{K}_{am}^- + \mathcal{K}_{ms}^-. \quad (41)$$

Using (41) and the first condition which is $\mathcal{K}_{ms}^+ > \mathcal{K}_{ms}^-$, the following can be obtained:

$$\mathcal{K}_{am}^+ < \mathcal{K}_{am}^-. \quad (42)$$

From (12) and the fact that $\mathcal{K}_{am} = \frac{1}{2} \dot{z}_a^\top M_a \dot{z}_a$, (42) can be written as

$$(\dot{z}_a^- + J_a^\dagger \delta V)^\top M_a (\dot{z}_a^- + J_a^\dagger \delta V) < \dot{z}_a^{-\top} M_a \dot{z}_a^-. \quad (43)$$

By applying the definition of J_a^\dagger , (43) can be further arranged as

$$\begin{aligned} (J_a \dot{z}_a^- + \delta V)^\top (J_a M_a^{-1} J_a^\top)^{-1} (J_a \dot{z}_a^- + \delta V) < \\ (J_a \dot{z}_a^-)^\top (J_a M_a^{-1} J_a^\top)^{-1} (J_a \dot{z}_a^-). \end{aligned} \quad (44)$$

Therefore, from Proposition 2 in appendix D and (44), there exist a positive constant L_c satisfying

$$\|\delta V\| < L_c \|J_a \dot{z}_a^-\| = L_c \|J_a \dot{z}_a^-\| \quad (45)$$

where the last equality comes from the second condition, $J_a \dot{z}_{a,d}^- = 0$.

Now, (45) can be applied to (33) as

$$\begin{aligned} |V_{m,1}(y_m^+) - V_{m,1}(y_m^-)| &\leq c_{m,0} V_{m,1}(y_m^-) + c_{m,1} L_c^2 \|J_a \dot{z}_a^-\|^2 \\ &< \tilde{c}_{m,0} V_{m,1}(y_m^-) + \tilde{c}_{m,1} \|\dot{\theta}^-\|^2 \end{aligned} \quad (46)$$

where the last inequality is derived from the fact that $\|J_a\|$ is bounded, $V_{m,1}(y_m)$ is quadratic, $y_m = [\tilde{z}_m; \dot{\tilde{z}}_m]$, and $\tilde{z}_a = [\tilde{z}_m; \dot{\theta}]$. $\tilde{c}_{m,0}, \tilde{c}_{m,1}$ are some positive scalars. Similarly, Lyapunov function analysis for controller state jump (37) can be arranged as

$$V_{m,2}(\tilde{\eta}_m^+) \leq \tilde{d}_{m,0} V_{m,2}(\tilde{\eta}_m^-) + \tilde{d}_{m,1} \|\dot{\theta}^-\|^2 + \tilde{d}_{m,2} \|\delta \lambda\|^2 \quad (47)$$

where $\tilde{d}_{m,0} > 1, \tilde{d}_{m,1} > 0$. Therefore, by combining (46) and (47), we can conclude the following:

$$V_m(x_m^+) \leq e^{\tilde{d}_m} V_m(x_m^-) + \tilde{d}_1 \|\dot{\theta}^-\|^2 + \tilde{d}_2 \|\delta \lambda\|^2 \quad (48)$$

where $\tilde{d}_m, \tilde{d}_1, \tilde{d}_2$ are some positive scalars. If we assume that an exogenous controller of the robotic arm provides $\dot{\theta}^- \approx 0$, the following holds for $FF \rightarrow FF$ jump

$$V_m(x_m^+) \leq e^{\tilde{d}_m} V_m(x_m^-),$$

and for $FF \rightarrow \{SPI, DPI\}$,

$$V_m(x_m^+) \leq e^{\tilde{d}_m} V_m(x_m^-) + \tilde{d}_2 \|\delta \lambda\|^2.$$

Jumps starting from *SPI* or *DPI* are omitted in the analysis since they are non-impulsive, and therefore, no δV exists originally.

Therefore, if nominal jump conditions are satisfied, taking rebounds ($FF \rightarrow FF$) for example, the end-effector velocity

jump δV no longer operates as perturbation. Note also that analysis without $\dot{\theta} \approx 0$ assumption is also possible if we construct a controller for the robotic arm dynamics (50) based on the same control law in (15).

VII. PUSHING STRATEGY

Sufficient amount of interaction force is required to push an object. However, since physical parameters of an interacting object, including mass and moment of inertia of the object, and friction between the ground and the object, are unknown, how large an interaction force should be to push an object is unknown. Furthermore, considering interaction with an object in an unstructured environment where an object may have kinematic constraints in certain direction or become stuck in-between pushing, the interaction force should be well regulated not to induce input saturation. Therefore, we choose a strategy of gradually increasing an interaction force until the object moves while decreasing the interaction force if encountering a maximum threshold for safety.

To implement this saturation-aware pushing strategy on top of a disturbance-rejecting robust motion controller, we modulate an end-effector position which indirectly controls the interaction force. Fig. 3 shows the three modes defined for this pushing strategy: APPROACH, PUSH, and RECOVER. $\lambda_{sn} \in \mathbb{R}$ is a surface-normal interaction force. During the APPROACH mode, an end-effector position setpoint is computed to approach towards a contact surface of the object. Then, whenever contact is stably established, which is represented as $\lambda_{sn} > \lambda_{A \rightarrow P}$ where $\lambda_{A \rightarrow P} > 0$, the mode changes to PUSH mode. In the PUSH mode, the end-effector position setpoint remains fixed. Thanks to the disturbance-rejecting property of the DOB-based robust controller, even small penetrating reference towards the contact surface can induce an increasing interaction force. Although continuously updating the position reference to further penetrate the contact surface would accelerate the increase rate of the interaction force as done in [5], such method may cause input saturation⁴ and show slower pitch angle stabilization in practice due to the time increase for the penetrated desired position to retract to the current position.

During experiments, non-ideal situation could occur where an aerial manipulator bumps into the contact surface during the APPROACH mode due to a distance measurement error between the end-effector and the contact surface. If such impact provokes rebound and activates a transition to the PUSH mode, since the setpoint is fixed during the PUSH mode, the aerial manipulator may fail to push the object. To overcome this problem, we allow a backward transition from the PUSH mode to the APPROACH mode when no interaction force is detected, which is represented as $\lambda_{sn} < \lambda_{P \rightarrow A}$. Here, $\lambda_{P \rightarrow A} > 0$ is a parameter small enough, and $\lambda_{P \rightarrow A} < \lambda_{A \rightarrow P}$

⁴This is because such update will accumulate a position error in the pushing direction so that even after the object moves, the desired pitch angle will still be tilted toward the pushing direction due to the enlarged position error. Since the motion of the object could incur sudden tangential friction loss on the contact surface, to overcome such friction loss which aided the aerial manipulator to maintain its pitch-tilt configuration, rotors related to pitch torque can get saturated.

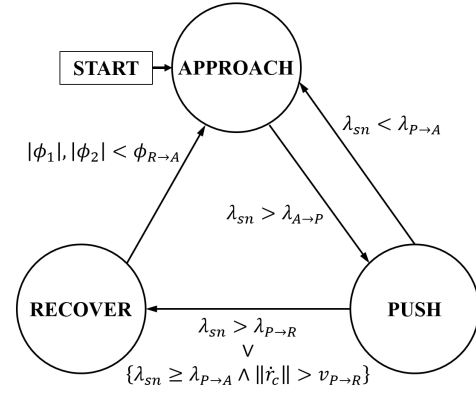


Fig. 3. Mode switching law in pushing strategy for APHl with a possibly dynamic object. $\lambda_{sn} \in \mathbb{R}$, $\phi, \dot{r}_c \in \mathbb{R}^3$ are surface-normal interaction force, Euler angles of the multirotor, and linear velocity of the multirotor, respectively.

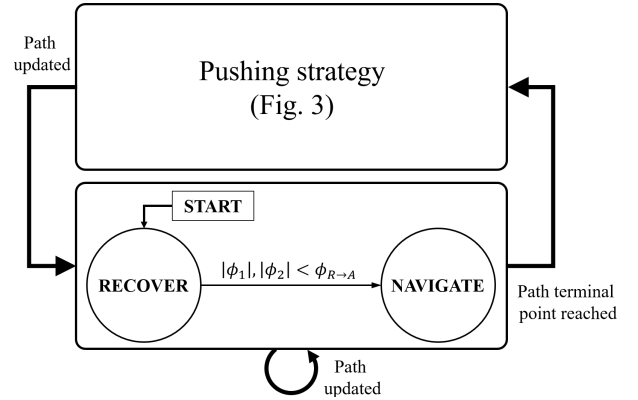


Fig. 4. Motion planner switching law. $\phi \in \mathbb{R}^3$ is Euler angle of the multirotor.

is assumed to avoid Zeno behavior [8] between A and P modes.

Next, we define the RECOVER mode to impose safety. During the RECOVER mode, the end-effector position setpoint is computed to retract backward against the pushing direction, inducing decrease in the interaction force. A transition from the PUSH mode to the RECOVER mode is activated only when 1) interaction force is excessively high $\lambda_{sn} > \lambda_{P \rightarrow R}$ or 2) the movable object starts to move $\{\lambda_{sn} \geq \lambda_{P \rightarrow A} \wedge \|\dot{r}_c\| > v_{P \rightarrow R}\}$. These two conditions are imposed to prevent input saturation due to excessive interaction force or sudden loss of contact in advance. We finish the RECOVER mode when the aerial manipulator starts to hover without interaction, and such condition is described as $|\phi_1|, |\phi_2| < \phi_{R \rightarrow A}$. To enable repetitive pushing, we define transition from the RECOVER mode to the APPROACH mode, whose transition condition is the terminating condition of the RECOVER mode. Note that although we terminate the pushing cycle, a cycle from APPROACH to PUSH to RECOVER and to APPROACH again, manually in current experiment setup, the pushing cycle can also be autonomously terminated by simply adding HOVER mode after the RECOVER mode and defining a terminate condition.

The pushing strategy assumes that the contact surface is

in front of the end-effector. To autonomously conduct APH with a possibly dynamic object in a more general setting including arbitrary initial position or sequential pushing while altering contact points, we integrate the pushing strategy with a high-level path planning algorithm. For smooth transition between the pushing strategy and the path navigating strategy, we introduce an intermediate RECOVER mode as in Fig. 4.

VIII. EXPERIMENTAL RESULTS

We consider the following five different experimental scenarios which contain uncertain discontinuities in both velocity and interaction wrench: pushing a possibly dynamic object

- 1) under unexpected change of friction,
- 2) while colliding with another movable object,
- 3) while colliding with a static environment,
- 4) on a slanted surface,
- 5) capable of both translation and rotation with multiple contacts.

The first, second, and fourth scenarios are presented to demonstrate robustness of the hybrid closed-loop system against uncertain discontinuities and continuous disturbance. The third scenario is to show effectiveness of the saturation-aware pushing strategy. We conduct the last scenario to investigate validity of the integrated motion planner combining the pushing strategy and a navigation algorithm to further applicability of an aerial manipulator in real world.

In all scenarios, we assume no knowledge of physical properties of a movable object such as mass, moment of inertia, friction coefficient, or restitution coefficient. The controller only requires state feedback, and the motion planner requires state feedback, pose of the contact surface, and interaction force. We utilize external motion capture system to obtain the pose of the contact surface and momentum-based wrench estimation algorithm [48] to estimate the interaction force. One may employ onboard sensors for estimating the pose of the contact surface, but we believe this is beyond the scope of the current study. An alternative of wrench estimation would be equipping a force/torque sensor at the end-effector as in [6, 23], but such strategy has a drawback of high cost and load increase. Although the estimated wrench through the momentum-based wrench estimator is a low-pass filtered signal of the true wrench [48], robust stability of the closed-loop system is still conserved since it is derived independently from the external wrench estimation.

A. Setup

We develop a tilt-hexarotor [27], a hexarotor with rotor mounts of fixed inclination (10° in our platform) to enable larger yaw torque generation. Note that although the utilized platform is fully actuated having 6-control degrees-of-freedom (cDoF), we utilize it as if it were 4 cDoF to directly apply the proposed controller. For physical interaction, a single cDoF robotic arm is attached to the tilt-hexarotor. As can be found in Fig. 10(a), we use an end-effector of dimension $25 \text{ cm} \times 5 \text{ cm}$.

For actuation of the tilt-hexarotor, we use six KDE rotors and two HOBBYWING ESCs, and for that of the robotic

TABLE II
PARAMETERS USED IN THE PLANNER AND CONTROLLER
(DIAGONAL ELEMENTS FOR MATRICES)

Parameter	Value	Parameter	Value
$\lambda_{A \rightarrow P}$	3.0 N	$v_{P \rightarrow R}$	0.07 m/s
$\lambda_{P \rightarrow R}$	20 N	\tilde{m}	2.9 kg
$\lambda_{P \rightarrow A}$	2.5 N	\tilde{J}	$10^{-2}[3.5, 3.5, 4.5] \text{ kgm}^2$
Gain	Value	Gain	Value
K_{up}	[6, 6]	K_{fp}	[8, 130, 130, 20]
K_{ud}	[4, 4]	K_{fd}	[5, 30, 30, 15]
ϵ_u	0.5	ϵ_f	0.1
$a_{0,u}, a_{1,u}$	1.0, 2.0	$a_{0,f}, a_{1,f}$	1.0, 2.0

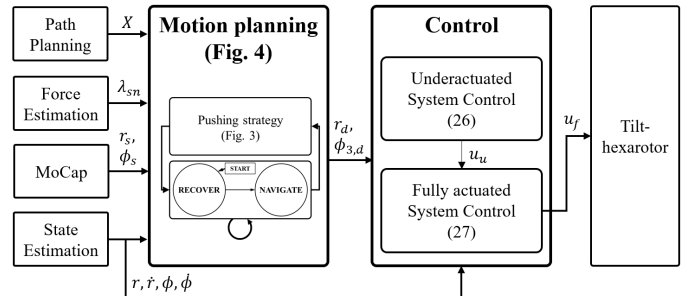


Fig. 5. Flow chart of the overall algorithms. The proposed algorithms, Motion planning and Control, are highlighted with boxes of thicker line, and auxiliary algorithms for experiments which are Path Planning, Force Estimation, and State Estimation are listed in the left.

arm, we use one ROBOTIS Dynamixel. The robotic arm is configured to rotate in the pitch direction so that the orientation of the end-effector remains aligned to the contact surface regardless of the pitching motion. Furthermore, to achieve the orientation alignment despite the rotation of the object being pushed, the motion planner computes the desired yaw angle $\phi_{3,d}$ according to the current orientation of the contact surface. OptiTrack motion capture system (MoCap) and LORD IMU are utilized for localization, and an error state Kalman filter [49] is applied to estimate the full state of the aerial robot. All algorithms including localization, control, and planning are executed in an onboard computer, Intel NUC, employing Robot Operating System (ROS) in Ubuntu 20.04.

Parameters and gains of the controller and the planner used during experiments are listed in Table II. Appropriate control gains are obtained from preliminary hovering experiments, and note that no additional fine tuning of control gains among experimental scenario change is conducted. Planning parameters $\lambda_{A \rightarrow P}$, $\lambda_{P \rightarrow A}$, $\lambda_{P \rightarrow R}$ are calculated from a preliminary cart pushing experiment in which setpoints r_d , $\phi_{3,d}$ shown in the overall flowchart Fig. 5 are generated manually instead. Note also that the planner parameters are fixed during all five experimental scenarios.

In Figs. 6–10, solid lines are either measured or estimated data, and dashed lines are desired trajectories. In all figures, the two graphs at the bottom show Euler angles of the aerial manipulator and an estimated interaction force during experiments. $\lambda_1, \lambda_2 \in \mathbb{R}$ in all figures are x, y -directional estimated interaction forces in a world fixed frame \mathcal{F}_W which is denoted in the captured image showing experimental results.

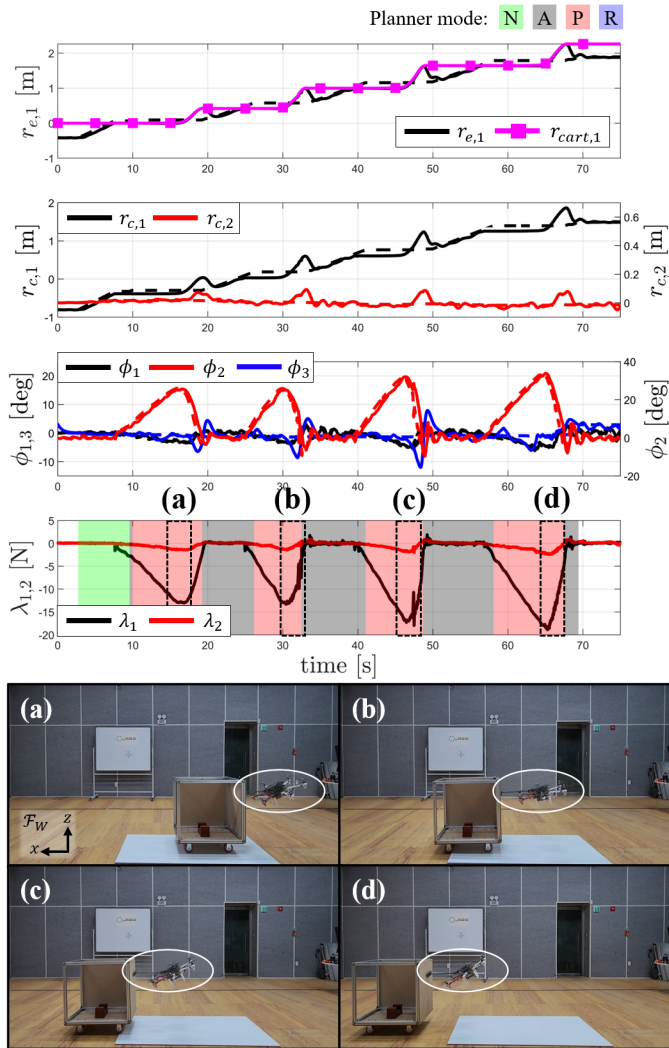


Fig. 6. Scenario 1 – Pushing a movable object under unexpected change of friction.

The background color of green, gray, red, and blue in the bottom graph indicates the planner mode each indicating NAVIGATE, APPROACH, PUSH, and RECOVER as in the top right legend of each graph. The graphs at the top in Figs. 6–9 show the end-effector position in the pushing direction $r_{e,1}$ and the contact surface position of the movable object $r_{cart,1}$, which is a cart. These graphs visualize when the movable object starts to move and when it halts. The graphs in the second row of Figs. 6–9 show x, y position of the aerial robot.

B. Scenario 1 – pushing a movable object under unexpected change of friction

In this scenario, an unidirectional movable cart is used as a movable object. Mass of the cart is about 30 kg including a 10 kg weight inside the cart, and four unidirectional casters are installed at the bottom of the cart. To provide different ground friction in the experiment, we lay a white wooden board on a brownish rubber mat as in Fig. 6. The white board provides smaller ground friction compared to the rubber mat. This friction change can also be inferred from the experimental

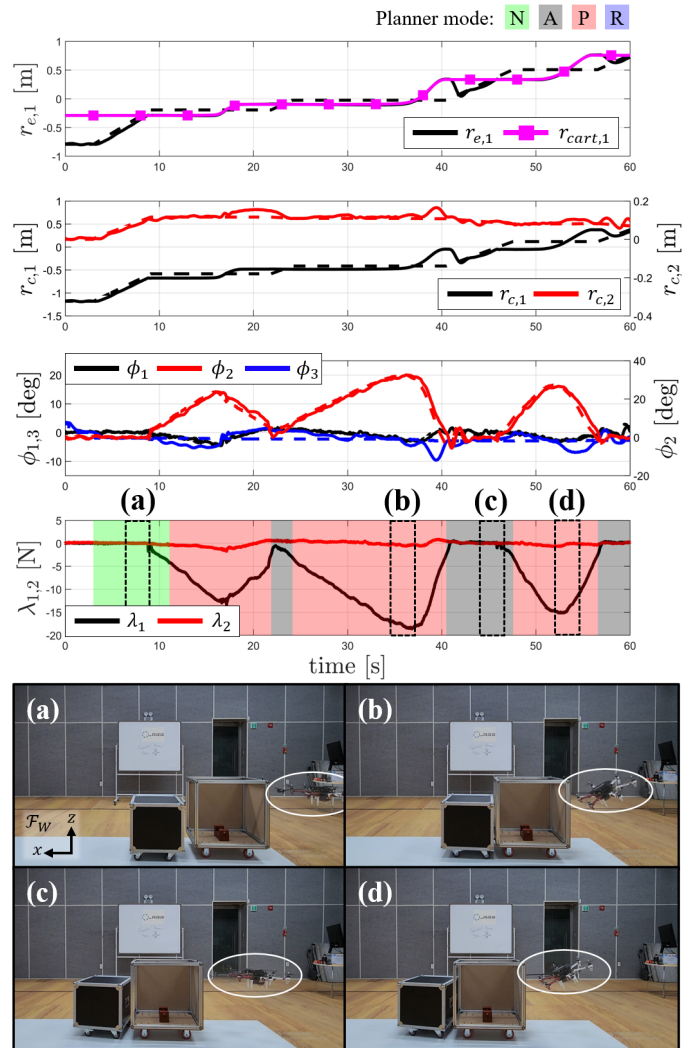


Fig. 7. Scenario 2 – Pushing a movable object while colliding with another movable object.

results in Fig. 6 where about 30 deg pitching is required when pushing the cart on the rubber mat while about 23 deg pitching only is required on the wooden board. In both ground conditions, and even during transitioning from the wooden board to the rubber mat, the controller could provide robust stability. Furthermore, consecutive cart pushing is successfully accomplished without the knowledge of the cart and the surrounding environment. Note also that the aerial robot shows robust stability against sudden contact-loss as guaranteed in Theorem 2 which occurs when the cart steps down from the wooden board to the rubber mat (between (b) and (c) in Fig. 6).

C. Scenario 2 – pushing a movable object while colliding with another movable object

This scenario is another demonstration of both robust stability of the controller and combined performance of the controller and planner eventually leading to successful pushing task. While being pushed, the cart encounters another unknown movable object, a black box in Fig. 7, and collides with it (see

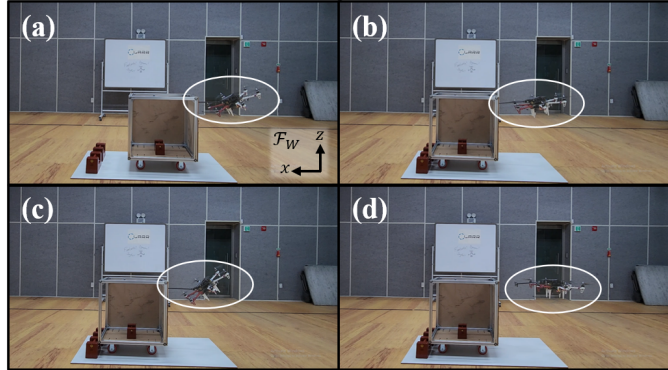
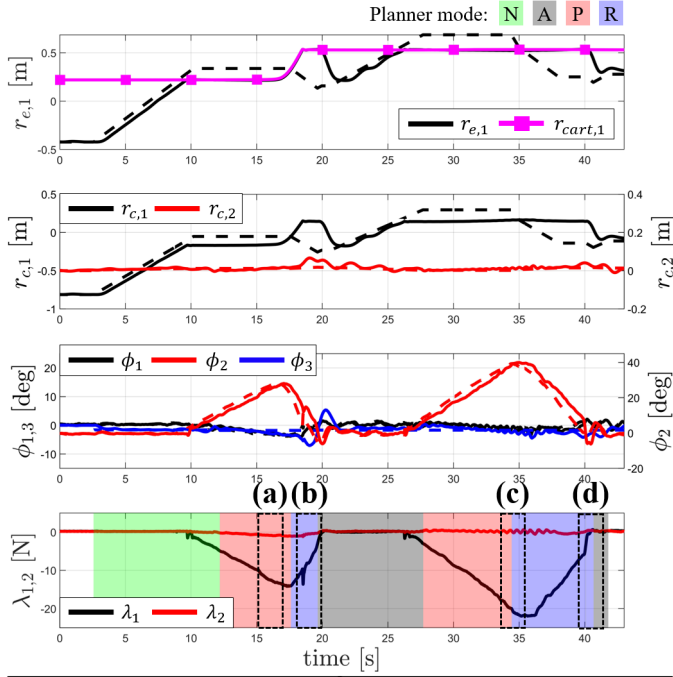


Fig. 8. Scenario 3 – Pushing a movable object while colliding with a static environment.

10–20 s in Fig. 7). Then, for a few moment during the second pushing (b), the black box moves jointly with the cart behaving as if it is an added mass to the cart. As the black box rotates and detaches from the cart as in (c), the aerial manipulator could push the cart with less endeavor (see lowered interaction force λ_1 at 54 s compared to that at 47 s during which the black box jointly moves with the cart). Through this experiment, we can conclude that robustness against sudden collision is validated, and the presented methods can succeed in pushing a movable object even when the mass of the object changes.

D. Scenario 3 – pushing a movable object while colliding with a static environment

While interacting with a movable object in an unstructured environment, it is plausible that the movable object collides with a static environment and stops to move. In this scenario, we validate that the applied safety condition $\lambda_{sn} > \lambda_{P \rightarrow R}$ in the pushing strategy in Fig. 3 can practically ensure safety. Since the aerial robot has no knowledge if the cart is static

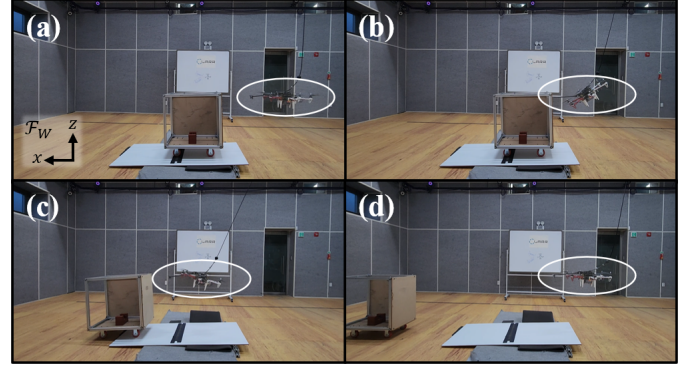
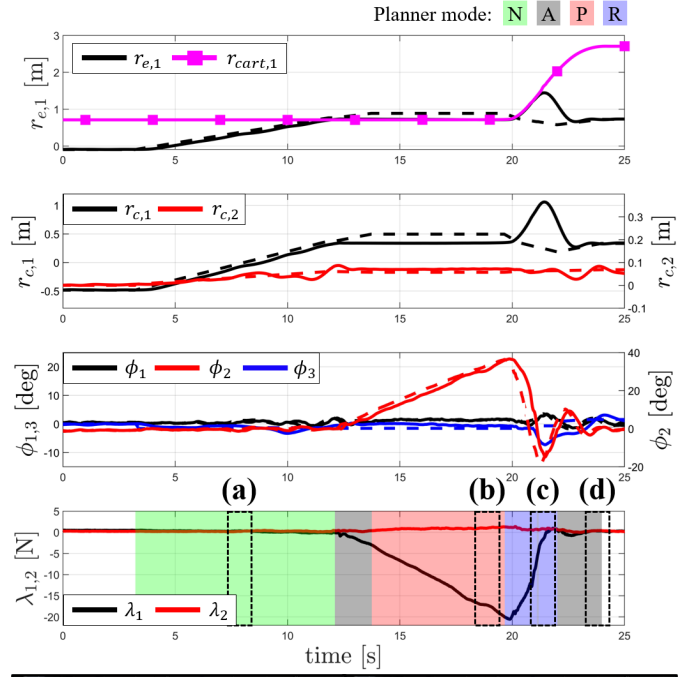


Fig. 9. Scenario 4 – Pushing a movable object on a slanted surface.

or movable, it first pushes the cart as in (a) of Fig. 8. During pushing, the cart collides with a static stopper as in (b). Then, as in (c), the aerial robot pushes the cart again, but due to the stopper behind the cart, the cart does not move. When the magnitude of the interaction force passes $\lambda_{P \rightarrow R}$ which is set to be 20 N, the RECOVER mode is again activated to provide safety. The robust stability is maintained during 40 deg of pitching. Thanks to this safety condition, APhI including collision with a static environment can be safely conducted.

E. Scenario 4 – pushing a movable object on a slanted surface

To test robustness against sudden contact-loss during APhI with a movable object, we conduct pushing a cart on a slanted surface as in Fig. 9. To make the cart be static on a slanted surface, we attach a black soft tape to the slanted surface and lay the front casters of the cart on the tape as in Fig. 9. Since the aerial robot does not know how much interaction force is required to push the cart, it gradually increases the pitch angle, which is the consequence of the controller and the planner. When the pitch angle reaches almost 40 deg, the cart starts to move, and due to the inclination, the cart slides down the

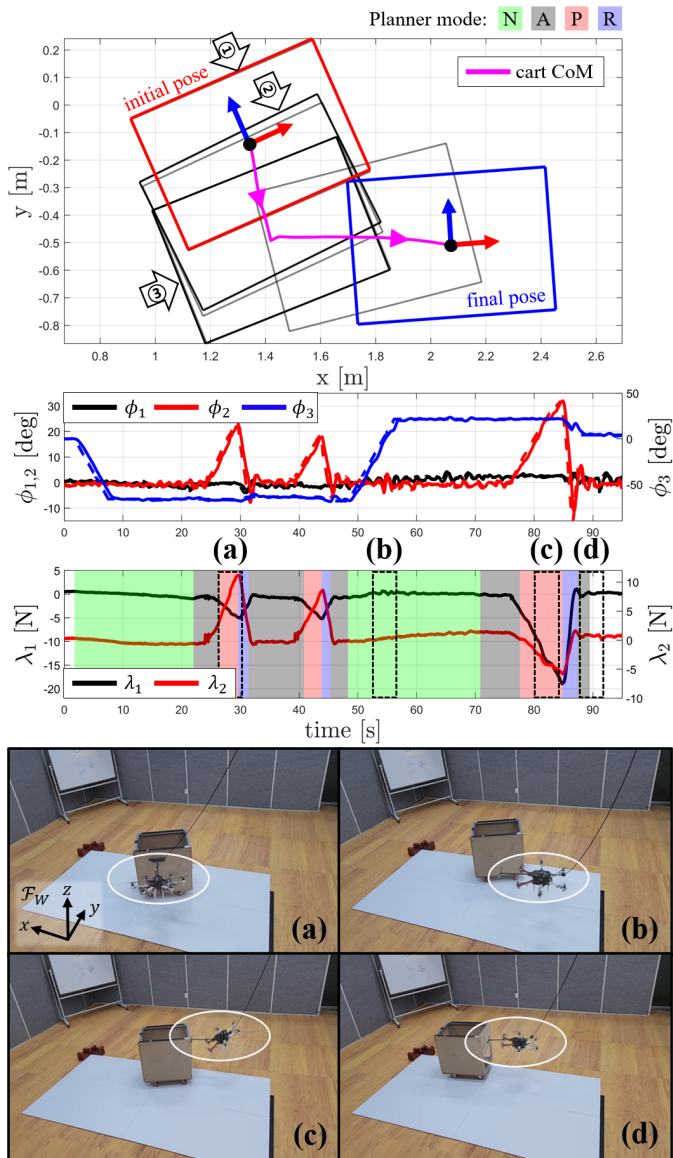


Fig. 10. Scenario 5 – Pushing a movable object capable of both translation and rotation with multiple contacts.

surface which results in sudden contact-loss. In the presence of such contact-loss, stable flight is still achieved as analyzed in Theorem 2.

F. Scenario 5 – pushing a movable object capable of both translation and rotation with multiple contacts

The last experiment is to show applicability of the proposed framework to pushing an omnidirectional movable object. For the experiment, we replace unidirectional casters to omnidirectional ones underneath the cart. Compared to other experiments conducted in [5–7] where only one directional motion of a movable object is considered, both translation and rotation should be properly tackled in this experiment, which makes the problem more challenging. Two major difficulties are 1) how much translation or rotation will occur varies as a contact point on the cart changes and 2) the same phenomenon can happen even for the same contact point since friction acting on each

caster changes over environment change. For example, despite the casters being omnidirectional, larger interaction force is required to push the cart if the casters are not aligned to the force direction. Since the cart is not only able to translate but also rotate after being pushed, collision between the aerial robot and the cart may happen after pushing. We found that the RECOVER strategy in the planner plays an important role in this collision avoidance since whenever the cart is pushed, the planner generates a retreating trajectory to avoid collision.

The experiment is conducted by first designating a desired contact surface on the cart. Then, the rest of the process is executed onboard and online: path planning, interaction force estimation, state estimation, motion planning, and control. The path planning module computes a collision-free path from the current position of the aerial manipulator to the designated contact point. An algorithmic flow can be found in Fig. 5. Whenever a new desired contact surface is designated by an operator, the same process from path planning to control is activated. The experimental result can be found in Fig. 10. Rectangles in the top graph visualize the pose of the cart at every 3 seconds. Arrows with numbers ①, ②, ③ indicate the three consecutive contact points. The experimental results validate the robustness of the proposed control and pushing strategy against unknown interaction wrench and unexpected motion of the omnidirectional cart which induces simultaneous force and torque disturbance to the aerial manipulator.

IX. CONCLUSION

In this work, we presented a hybrid system analysis of aerial physical interaction to guarantee robustness against sufficiently smooth disturbance and a class of discontinuous uncertainties including collision and contact-loss. To achieve the analysis, we first derived a hybrid system model of APhI with a movable object and transformed the closed-loop dynamics into impulsive switched system where a nonlinear DOB-based controller was applied. Robustness of each continuous dynamics and discrete dynamics was analyzed, and that of the overall closed-loop impulsive switched system was verified by applying the derived stability condition for an impulsive switched system with multiple discrete dynamics. We also proposed a motion planning to enable APhI while providing practical safety with respect to rotor saturation which could be incurred by large interaction wrench or sudden contact-loss that induces large torque generation to compensate the vanished friction. We employed a finite state machine where multiple modes and switching law among them are defined. To validate the proposed framework, comprehensive experiments were successfully demonstrated using an underactuated aerial manipulator: 1) pushing a movable object with a sudden ground friction change, 2) with a sudden collision with another movable object, 3) with a sudden collision with a static environment, 4) with a sudden contact-loss, and 5) pushing an omnidirectional movable object with multiple contacts.

Transporting a movable object to a target position and orientation by pushing is not the objective of the current work. Such a task is addressed in the ongoing research area of *Nonprehensile pushing manipulation*, which has been mainly

studied for ground mobile robots [50–54]. Incorporating such pushing manipulation strategies as a high-level planner into our framework could be an interesting research direction.

APPENDIX

A. Proof of Theorem 1

Proof. The difference between [35, Theorem 1] and this theorem is that this theorem additionally includes multiple models in discrete dynamics. By imposing the same inequality condition (4c) to all $\{g_i : i \in l_d\}$, the same ISS result can be obtained by following the proof of [40, Theorem 1]. Conditions of [40, Theorem 1] can be shown to be satisfied by choosing $\lambda = c - d/\tau_D$ and $0 < \mu \leq N_0 d$ if $d > 0$, and any arbitrary $0 < \lambda < c$, $\mu > 0$ if $d < 0$. \square

B. Derivation of robotic arm dynamics

From (6b), robotic arm dynamics can be derived as

$$M_\theta \ddot{\theta} + C_\theta = B_\theta u_a + \delta_\theta - M_{\phi\theta}^\top \ddot{\phi} \quad (49)$$

where $u_a = [T; \tau_\phi; \tau_\theta]$, $B_\theta = [S_\theta^\top Re_3 \quad 0_{m \times 3} \quad I_m]$. A definition of $S_\theta \in \mathbb{R}^{3 \times m}$ can be found in appendix C. Then, the robotic arm dynamics can be computed as

$$\ddot{\theta} = F_\theta + G_\theta u_\theta + \Delta_\theta \quad (50)$$

where $F_\theta = -M_\theta^{-1} C_\theta$, $G_\theta = M_\theta^{-1}$, $\Delta_\theta = M_\theta^{-1} (J_\theta^\top \lambda_a + \delta_\theta - M_{\phi\theta}^\top \ddot{\phi} + S_\theta^\top Re_3 T)$, $u_\theta = \tau_\theta$.

C. Definition of S_ϕ , S_θ

To define S_ϕ, S_θ which originate from coordinate transformation appeared in [42], we first introduce a new generalized coordinate $z_n = [r; \phi; \theta] \in \mathbb{R}^{6+m}$ where r is the CoM position of the multirotor. Then, using an Euler-Lagrange equation, equations of motion of the aerial manipulator can be derived as

$$M_n \ddot{z}_n + C_n \dot{z}_n + G_n = B_n u_a + \delta_n$$

where $u_a = [T; \tau_\phi; \tau_\theta]$. Defining submatrices of M_n as $M_{n,11} \in \mathbb{R}^{3 \times 3}$, $M_{n,12} \in \mathbb{R}^{3 \times (3+m)}$, $M_{n,22} \in \mathbb{R}^{(3+m) \times (3+m)}$ satisfying

$$M_n = \begin{bmatrix} M_{n,11} & M_{n,12} \\ M_{n,12}^\top & M_{n,22} \end{bmatrix},$$

S_ϕ, S_θ are defined from $[S_\phi \quad S_\theta] = -M_{n,11}^{-1} M_{n,12}$.

D. Proposition 2 and proof

Proposition 2. *Given a symmetric, positive definite matrix $A > 0$, if $(x + v)^\top A(x + v) < v^\top A v$, then there exist a constant $L_c > 0$ such that $0 < \|x\| < L_c \|v\|$.*

Proof. Since A is positive-definite, there exist positive scalars $\underline{\lambda}, \bar{\lambda} > 0$ satisfying $\underline{\lambda} I \leq A \leq \bar{\lambda} I$. Therefore, using the triangle inequality, $\underline{\lambda} (\|x\|^2 - \|v\|^2) < \bar{\lambda} \|v\|^2$. The proof is finished by taking $L_c = \sqrt{\bar{\lambda}/\underline{\lambda}} + 1$. \square

REFERENCES

- [1] A. Ollero, M. Tognon, *et al.*, “Past, present, and future of aerial robotic manipulators,” *IEEE Trans. Robot.*, vol. 38, no. 1, pp. 626–645, 2022.
- [2] F. Ruggiero, V. Lippiello, and A. Ollero, “Aerial manipulation: A literature review,” *IEEE Robot. Autom. Lett.*, vol. 3, no. 3, pp. 1957–1964, 2018.
- [3] J. W. Grizzle, C. Chevallereau, *et al.*, “Models, feedback control, and open problems of 3d bipedal robotic walking,” *Automatica*, vol. 50, no. 8, pp. 1955–1988, 2014.
- [4] L. Marconi, R. Naldi, and L. Gentili, “Modelling and control of a flying robot interacting with the environment,” *Automatica*, vol. 47, no. 12, pp. 2571–2583, 2011.
- [5] D. Lee, H. Seo, *et al.*, “Aerial manipulator pushing a movable structure using a dob-based robust controller,” *IEEE Robot. Autom. Lett.*, vol. 6, no. 2, pp. 723–730, 2021.
- [6] F. Benzi, M. Brunner, *et al.*, “Adaptive tank-based control for aerial physical interaction with uncertain dynamic environments using energy-task estimation,” *IEEE Robot. Autom. Lett.*, vol. 7, no. 4, pp. 9129–9136, 2022.
- [7] M. Brunner, L. Giacomini, *et al.*, “Energy tank-based policies for robust aerial physical interaction with moving objects,” in *2022 IEEE Int. Conf. Robot. Autom.* IEEE, 2022, pp. 2054–2060.
- [8] R. Goebel, R. G. Sanfelice, and A. R. Teel, “Hybrid dynamical systems,” *IEEE Control Syst. Mag.*, vol. 29, no. 2, pp. 28–93, 2009.
- [9] P. M. Wensing, M. Posa, *et al.*, “Optimization-based control for dynamic legged robots,” *IEEE Trans. Robot.*, 2023.
- [10] G. Darivaniakis, K. Alexis, *et al.*, “Hybrid predictive control for aerial robotic physical interaction towards inspection operations,” in *2014 IEEE Int. Conf. Robot. Autom.* IEEE, 2014, pp. 53–58.
- [11] J. Byun, D. Lee, *et al.*, “Stability and robustness analysis of plug-pulling using an aerial manipulator,” in *2021 IEEE/RSJ Int. Conf. Intell. Robots Syst.* IEEE, 2021, pp. 4199–4206.
- [12] H. Nguyen and K. Alexis, “Forceful aerial manipulation based on an aerial robotic chain: Hybrid modeling and control,” *IEEE Robot. Autom. Lett.*, vol. 6, no. 2, pp. 3711–3719, 2021.
- [13] W.-L. Ma, K. A. Hamed, and A. D. Ames, “First steps towards full model based motion planning and control of quadrupeds: A hybrid zero dynamics approach,” in *2019 IEEE/RSJ Int. Conf. Intell. Robots Syst.* IEEE, 2019, pp. 5498–5503.
- [14] K. A. Hamed, W.-L. Ma, and A. D. Ames, “Dynamically stable 3d quadrupedal walking with multi-domain hybrid system models and virtual constraint controllers,” in *2019 Am. Control Conf.* IEEE, 2019, pp. 4588–4595.
- [15] A. D. Ames, K. Galloway, *et al.*, “Rapidly exponentially stabilizing control lyapunov functions and hybrid zero dynamics,” *IEEE Trans. Autom. Control*, vol. 59, no. 4, pp. 876–891, 2014.
- [16] M. Brunner, G. Rizzi, *et al.*, “A planning-and-control framework for aerial manipulation of articulated objects,” *IEEE Robot. Autom. Lett.*, vol. 7, no. 4, pp. 10689–10696, 2022.
- [17] D. Lee, H. Seo, *et al.*, “Aerial manipulation using model predictive control for opening a hinged door,” in *2020 IEEE Int. Conf. Robot. Autom.* IEEE, 2020, pp. 1237–1242.
- [18] M. Zhao, K. Nagato, *et al.*, “Forceful valve manipulation with arbitrary direction by articulated aerial robot equipped with thrust vectoring apparatus,” *IEEE Robot. Autom. Lett.*, vol. 7, no. 2, pp. 4893–4900, 2022.
- [19] S. Kim, H. Seo, and H. J. Kim, “Operating an unknown drawer using an aerial manipulator,” in *2015 IEEE Int. Conf. Robot. Autom.* IEEE, 2015, pp. 5503–5508.
- [20] X. Meng, Y. He, and J. Han, “Design and implementation of a contact aerial manipulator system for glass-wall inspection tasks,” in *2019 IEEE/RSJ Int. Conf. Intell. Robots Syst.* IEEE, 2019, pp. 215–220.
- [21] C. Papachristos, K. Alexis, and A. Tzes, “Efficient force exertion for aerial robotic manipulation: Exploiting the thrust-vectoring authority of a tri-tiltrotor uav,” in *2014 IEEE Int. Conf. Robot. Autom.* IEEE, 2014, pp. 4500–4505.
- [22] H. W. Wopereis, W. L. Van De Ridder, *et al.*, “Multimodal aerial locomotion: An approach to active tool handling,” *IEEE Robot. Autom. Mag.*, vol. 25, no. 4, pp. 57–65, 2018.
- [23] K. Bodie, M. Brunner, *et al.*, “Active interaction force control for contact-based inspection with a fully actuated aerial vehicle,” *IEEE Trans. Robot.*, vol. 37, no. 3, pp. 709–722, 2021.
- [24] D. Tzoumanikas, F. Graule, *et al.*, “Aerial manipulation using hybrid force and position nmpc applied to aerial writing,” *Proceedings of Robotics: Science and Systems XVI*, 2020.

- [25] C. Ding, L. Lu, *et al.*, “Design, sensing, and control of a novel uav platform for aerial drilling and screwing,” *IEEE Robot. Autom. Lett.*, vol. 6, no. 2, pp. 3176–3183, 2021.
- [26] G. Nava, Q. Sablé, *et al.*, “Direct force feedback control and online multi-task optimization for aerial manipulators,” *IEEE Robot. Autom. Lett.*, vol. 5, no. 2, pp. 331–338, 2020.
- [27] M. Ryll, G. Muscio, *et al.*, “6d interaction control with aerial robots: The flying end-effector paradigm,” *Int. J. Robot. Res.*, vol. 38, no. 9, pp. 1045–1062, 2019.
- [28] R. Naldi, A. Macchelli, *et al.*, “Robust control of an aerial manipulator interacting with the environment,” *IFAC-PapersOnLine*, vol. 51, no. 13, pp. 537–542, 2018.
- [29] J. Liang, Y. Chen, *et al.*, “Low-complexity prescribed performance control for unmanned aerial manipulator robot system under model uncertainty and unknown disturbances,” *IEEE Trans. Industr. Inform.*, vol. 18, no. 7, pp. 4632–4641, 2022.
- [30] S. Kim, S. Choi, *et al.*, “Robust control of an equipment-added multi-rotor using disturbance observer,” *IEEE Trans. Control Syst. Technol.*, vol. 26, no. 4, pp. 1524–1531, 2017.
- [31] H. Lee and H. J. Kim, “Estimation, control, and planning for autonomous aerial transportation,” *IEEE Trans. Ind. Electron.*, vol. 64, no. 4, pp. 3369–3379, 2016.
- [32] J. Byun, I. Jang, *et al.*, “A hybrid controller enhancing transient performance for an aerial manipulator extracting a wedged object,” *IEEE Trans. Autom. Sci. Eng.*, 2023.
- [33] C. Wu, J. Zhao, and X.-M. Sun, “Adaptive tracking control for uncertain switched systems under asynchronous switching,” *Int. J. Robust Nonlinear Control*, vol. 25, no. 17, pp. 3457–3477, 2015.
- [34] X. Li, P. Li, and Q.-g. Wang, “Input/output-to-state stability of impulsive switched systems,” *Syst. Control Lett.*, vol. 116, pp. 1–7, 2018.
- [35] J. P. Hespanha, D. Liberzon, and A. R. Teel, “Lyapunov conditions for input-to-state stability of impulsive systems,” *Automatica*, vol. 44, no. 11, pp. 2735–2744, 2008.
- [36] J. Liu, X. Liu, and W.-C. Xie, “Class-kl estimates and input-to-state stability analysis of impulsive switched systems,” *Syst. Control Lett.*, vol. 61, no. 6, pp. 738–746, 2012.
- [37] S. Hong and Y. Zhang, “Input/output-to-state stability of impulsive switched delay systems,” *Int. J. Robust Nonlinear Control*, vol. 29, no. 17, pp. 6031–6052, 2019.
- [38] D. Liberzon, *Switching in systems and control*. Springer Science & Business Media, 2003.
- [39] E. D. Sontag and Y. Wang, “On characterizations of the input-to-state stability property,” *Syst. Control Lett.*, vol. 24, no. 5, pp. 351–359, 1995.
- [40] J. P. Hespanha and A. S. Morse, “Stability of switched systems with average dwell-time,” in *Proc. IEEE Conf. Decis. Control*, vol. 3. IEEE, 1999, pp. 2655–2660.
- [41] B. Brogliato, *Nonsmooth Mechanics*. Springer, 2016.
- [42] H. Yang and D. Lee, “Dynamics and control of quadrotor with robotic manipulator,” in *2014 IEEE Int. Conf. Robot. Autom.* IEEE, 2014, pp. 5544–5549.
- [43] J. Liang, Y. Chen, *et al.*, “Adaptive prescribed performance control of unmanned aerial manipulator with disturbances,” *IEEE Trans. Autom. Sci. Eng.*, vol. 20, no. 3, pp. 1804–1814, 2023.
- [44] D. Lee, J. Byun, and H. J. Kim, “Rise-based trajectory tracking control of an aerial manipulator under uncertainty,” *IEEE Control Syst. Lett.*, vol. 6, pp. 3379–3384, 2022.
- [45] J. Moreno-Valenzuela, R. Pérez-Alcocer, *et al.*, “Nonlinear pid-type controller for quadrotor trajectory tracking,” *IEEE/ASME Transactions on Mechatronics*, vol. 23, no. 5, pp. 2436–2447, 2018.
- [46] J. Back and H. Shim, “An inner-loop controller guaranteeing robust transient performance for uncertain mimo nonlinear systems,” *IEEE Trans. Autom. Control*, vol. 54, no. 7, pp. 1601–1607, 2009.
- [47] H. K. Khalil and J. W. Grizzle, *Nonlinear systems*. Prentice hall Upper Saddle River, NJ, 2002, vol. 3.
- [48] T. Tomić, C. Ott, and S. Haddadin, “External wrench estimation, collision detection, and reflex reaction for flying robots,” *IEEE Trans. Robot.*, vol. 33, no. 6, pp. 1467–1482, 2017.
- [49] [Online]. Available: https://github.com/ChanghyeonKim93/error_state_kalman_filter_ros
- [50] F. Bertonecchi, F. Ruggiero, and L. Sabattini, “Linear time-varying mpc for nonprehensile object manipulation with a nonholonomic mobile robot,” in *2020 IEEE Int. Conf. Robot. Autom.* IEEE, 2020, pp. 11 032–11 038.
- [51] A. Rigo, Y. Chen, *et al.*, “Contact optimization for non-prehensile loco-manipulation via hierarchical model predictive control,” in *2023 IEEE Int. Conf. Robot. Autom.* IEEE, 2023, pp. 9945–9951.
- [52] Y. Tang, H. Zhu, *et al.*, “Unwieldy object delivery with nonholonomic mobile base: A stable pushing approach,” *IEEE Robot. Autom. Lett.*, vol. 8, no. 11, pp. 7727–7734, 2023.
- [53] A. Heins and A. P. Schoellig, “Force push: Robust single-point pushing with force feedback,” *arXiv preprint arXiv:2401.17517*, 2024.
- [54] I. Ozdamar, D. Sirintuna, *et al.*, “Pushing in the dark: A reactive pushing strategy for mobile robots using tactile feedback,” *arXiv preprint arXiv:2403.09305*, 2024.



Dongjae Lee (Graduate Student Member, IEEE) received the B.S. and M.S. degrees in mechanical and aerospace engineering in 2018 and 2020, respectively, from Seoul National University, Seoul, South Korea, where he is currently working toward the Ph.D. degree in aerospace engineering.

His current research interests include control and planning of robotic systems.



Jeonghyun Byun (Graduate Student Member, IEEE) received the B.S. degree in aerospace engineering in 2020 from Seoul National University, Seoul, South Korea, where he is currently pursuing the Ph.D. degree in aerospace engineering.

His current research interests include control and planning of aerial robots.



Hyoun Jin Kim (S'98-M'02) received the B.S. degree from the Korea Advanced Institute of Technology, Daejeon, South Korea, in 1995, and the M.S. and Ph.D. degrees in mechanical engineering from the University of California at Berkeley (UC Berkeley), Berkeley, CA, USA, in 1999 and 2001, respectively.

From 2002 to 2004, she was a Post-Doctoral Researcher in electrical engineering and computer science with UC Berkeley. In 2004, she joined the Department of Mechanical and Aerospace Engineering, Seoul National University, Seoul, South Korea, as an Assistant Professor, where she is currently a Professor. Her current research interests include intelligent control of robotic systems and motion planning.